Fall 2018

# Late Holocene Spit Evolution on Centennial Timescales in the Southeast Delaware Bay, USA

Ryan Eli Phillip
*Coastal Carolina University*

Follow this and additional works at: https://digitalcommons.coastal.edu/etd

Part of the Geology Commons, and the Sedimentology Commons

LATE HOLOCENE SPIT EVOLUTION ON CENTENNIAL TIMESCALES IN THE

SOUTHEAST DELAWARE BAY, USA

By

Ryan Eli Phillip

Submitted in Partial Fulfillment of the

Requirements for the Degree of Master of Science in

Coastal Marine and Wetland Studies in the

School of Coastal and Marine Systems Science

Coastal Carolina University

2018

| | |
|---|---|
| _____ | _____ |
| Dr. Zhixiong Shen, Major Professor | Dr. Eric Wright |
| _____ | _____ |
| Dr. Shaowu Bao | Dr. Michael H. Roberts, Dean |
| _____ | |
| Dr. Richard F. Viso, SCMSS Director | |

**Acknowledgements**

**Abstract**

The relationship between barrier spit growth and longshore drift is well established. However, the role of storm activity in spit evolution on an intermediate (centennial) timescale is more of a mystery due to a knowledge gap between decadal-scale shoreline processes and millennial-scale stratigraphic data. Recent studies in the northwestern Atlantic basin using ground-penetrating radar (GPR) and optically-stimulated luminescence (OSL) are providing the opportunity to study centennial-scale shoreline evolution and examine similar age storm activity. Cape Henlopen, Delaware exhibits preserved remnants of a long-term northward-growing spit coastline that evolved from a recurved spit complex, to a cuspate spit, to the present-day simple spit. This location provides ideal late-Holocene spit features on which to collect GPR and OSL data. Within Cape Henlopen State Park, approximately 10 trackline-km of GPR data were collected from the southernmost relict recurved spits to the more northern simple spit for the purpose of revealing the internal architecture and growth patterns of the spits, as well as evidence of storm influence. A total of 8 OSL samples were obtained to find coincidences among the ages of the spit deposits and periods of increased storm activity. GPR analysis exhibits 5 major sedimentary facies: shallow marine, spit platform, spit beach and dune, overwash fan foreset deposits, and modern dunes. OSL ages indicate that spit development began around 2.4 ka, followed by phases of major growth of recurved spits during CE 100 to 500 (1.9-1.5 ka) and then converting to a cuspate foreland around CE 1500 (0.5 ka). Analysis of the OSL dates reveals concurrences between the ages of the spit features and periods of increased storm frequency during CE 0 to 700 (2.0-1.3 ka) and CE 1300 to 1800(0.7-0.2 ka) in the North Atlantic basin which produces evidence that storm activity may have a significant influence on barrier spit evolution on centennial timescales. The results of this study provide both an increased understanding of how barrier spits evolve as well as centennial-scale data to be used for coastal change and hazard management modeling.

**Table of Contents**

**Table of Figures**

# 1    Introduction

Nearly 40 percent of the United States population resides in coastal localities affected by flooding, shoreline erosion, and storm hazards; all of which increasing in intensity and frequency with rising sea levels (NOAA, 2017). To better predict and plan for such hazards, an improved understanding of the formation of natural coastal features is required. More specifically, how coastal features such as spits form and grow.

However, there is currently a lack of intermediate- (centennial) scale data required for coastal hazard prediction and management modeling (Dougherty et al., 2016). This deficiency is due to a knowledge gap between decadal-scale shoreline processes and millennial-scale stratigraphic data. Dougherty et al. (2016) proposes the application of ground-penetrating radar (GPR) in conjunction with optically-stimulated luminescence (OSL) age dating for closing the aforementioned knowledge gap.

Coastal barrier spits are common geomorphic features along the United States Atlantic and Gulf coasts. Despite their seemingly small geographic dimensions, spits are economically, ecologically, and geologically important to our coastlines. Spits provide natural storm protection, are crucial for fish and shellfish industries, are a unique habitat for a variety of organisms, and can hold geological archives of both distant and recent coastal history. Barrier spits are highly dynamic coastal features, which makes studying their sedimentology and evolution difficult. Deciphering barrier spit evolution, however, can contribute in the understanding of long-term shoreline processes (Costas and FitzGerald, 2011), historic tempest occurrence, and response of barrier spits to storms. A spit is defined as a detrital depositional feature, composed of sand or shingle, that protrudes off of an eroding headland coast (Davis, 1896; Ashton et al., 2016). Spits are typically

narrow near the headland and backed by embayments and backbarrier marshes (Schwartz, 1972), with a curved end consisting of sub-parallel ridges as a result of progradation (Ashton et al., 2016). Spit growth and direction has traditionally been attributed to longshore sediment transport via littoral currents (Gilbert, 1885; Evans, 1939; Bruun, 1953; Zenkovitch, 1967) fed by updrift eroding headlands (Gulliver, 1899; Johnson, 1919).

Many barrier spits occur at the mouth of bays and inlets. Initial development of a spit environment begins with deposition of what has been termed the spit platform (Meistrell, 1972; Moslow and Heron, 1978; Costas and FitzGerald, 2011). The spit platform is essentially a subaqueous embankment that forms by sediment accretion of the updrift inlet margin (Moslow and Heron, 1978). Sediment supply and water depth controls spit platform growth; a larger volume of sediment is needed to fill the accommodation space as the spit platform grows into deeper water, which results in the spit elongating at a slower rate (King and McCullagh, 1971; Costas et al., 2015).

The spit itself is a partially emergent ridge that develops, similarly to the platform, through sediment accretion of the updrift inlet margin on top of the spit platform (Moslow and Heron, 1978; Costas and FitzGerald, 2011; Avinash et al., 2013; Costas et al., 2015). Since spits are typically narrow near the eroding headland, they are prone to overwash. (Petersen et al., 2008; Ashton et al., 2016). This narrow region is erosive and comprises the neck of the spit which extends from the headland to the location of maximum sediment transport (Ashton et al., 2016). Overwash is responsible for landward sediment exchange and is the main factor for the evolution of the inner coast of the spit (Leatherman, 1979; Héquette and Ruz, 1991; Jiménez and Sánchez-Arcilla, 2004; Costas et al., 2006; Avinash et al., 2013). Barrier spit width and topography, back-barrier lagoon depth and size, and

type of storm are the major factors that influence the formation of a washover fan or tidal inlet (Pierce, 1970; Leatherman, 1979). Sediment may be transported from an ebb-tidal delta and deposited on adjacent beaches (e.g. spit beaches) when wave energy is higher than normal (Kana et al., 1999). Spit ends are usually curved and characterized by recurved ridges formed due to wave refraction as waves propagate through the inlet and into the backbarrier zone (Gilbert, 1885; Evans, 1939; Bruun, 1953; King and McCullagh, 1971; Hine 1979; Simms et al., 2006; Costas and FitzGerald, 2011; Ashton et al., 2016;). The point between the neck and the spit end where sediment transport is maximized and erosion transitions to accretion is defined as the fulcrum point (Davis, 1896; Ashton et al., 2016).

Swash bars may also be incorporated into a spit's morphology. Swash-bar sedimentation is wave-induced and related to beach recovery both during and after storm events (Bristow et al., 2000; Dougherty et al., 2004; Houser and Greenwood, 2007; Lindhorst et al., 2008; Costas and FitzGerald, 2011). Attachment of swash bars to the barrier spit is episodic and seems to follow erosional events. Costas and FitzGerald (2011) suggests that both storms and the onshore migration of the swash bar itself are potential mechanisms of the erosional events. It is also suggested that swash-bar welding dominates the process of spit elongation in stable inlets (Hine, 1979; Costas and FitzGerald, 2011).

Wave climate affects both the shape and trajectory of a spit. Models produced by Ashton et al. (2016) suggest that even a small change in the wave angle distribution can move the fulcrum point, essentially moving the transition point between the erosional neck and the accretionary hook. Waves, particularly wave angles, also significantly affect longshore sediment transport. Wave angles near 45° transport larger fluxes of sediment whereas wave angles near 0° or 90° transport much smaller fluxes of sediment (Bruun,

1953; Ashton et al., 2016). However, Petersen et al. (2008) produced an analytical model suggesting that a growing spit fed by longshore transport with no retreat of the shoreline along the spit requires the dominant waves approaching the coast at an angle larger than 45°. These highly oblique waves are associated with unstable coastlines that form features such as spit fingers and competing spits that overtake each other (Ashton et al., 2001; Petersen et al., 2008; Thomas et al., 2014). Ashton and Murray (2006b) note that the influence of high-angle waves can be obscured by scale; high-angle waves may shape large-scale coastal features while low-angle waves seem more prominent upon local examination.

The basin depth in which a spit is prograding into also plays a role in its morphology. Progradation into deeper waters is slower than that into shallower waters (Costas et al., 2015); however, models show that spits growing into deeper waters may have much smaller hook lengths while reduction in neck growth rate is small (Ashton et al., 2016). A sharper curvature of the spit hook is required for the spit to extend at the same rate while prograding into deeper water since the same sediment influx must be dispersed over a greater depth (Ashton et al., 2016).

Additionally, barrier spits may be affected by tidal deltas. Tidal inlet sediments may compose 30-60% of the sediments deposited in barrier island complexes (Moslow and Heron, 1978; Hayes, 1979, 1980; Aubrey and Gaines, 1982). Mallinson et al. (2010) states that flood-tide delta deposits compose a significant volume of the spit platform beneath the Outer Banks. An ebb-tidal delta is an accumulation of sediment that forms seaward of an inlet from deposition by ebb-tidal currents interacting with waves (Hayes, 1969, 1980; Imperato et al., 1988). Waves refracting around ebb-tidal deltas are partially responsible

for the widening and curving of the head of spits in mesotidal environments (Hayes, 1979). At the seaward end of the main ebb channel in a tidal inlet lies the ebb-tidal delta terminal lobe which is a moderately steep, seaward-sloping lobe of sand. The sands composing the terminal lobe can be pushed onshore via wave action if the main ebb channel abandons a downdrift course for a more updrift course (Hayes, 1979). This process may be associated with the process of swash bar welding mentioned earlier.

While longshore transport is the primary mechanism for spit progradation, external forces (e.g. storms) are responsible for moving sediment from the foreshore to the shoreface (Lindhorst et al., 2010). Increased winds and waves caused by storms result in an increase in sediment movement that contributes to spit growth (Thomas et al., 2014). Avinash et al. (2013) found that monsoon-influenced currents and longshore drifts are the primary processes for the formation and growth of the Uliyargoli-Padukere, Oddu Bengre, and Kodi Bengre spits in southern Karnataka, India. In a different study, Allard et al. (2008) determined that at a longer time scale (centennial) the growth of the Arçay Spit on the French Atlantic coast is associated with periods of energetic swells or high storm surge frequency in relation to wave climate variations.

In regard to internal forcing, modeling of spit evolution has revealed an important feedback system between spit extension and the headland. For example, a narrow, quickly eroding headland reduces the rate of headland sediment loss and the rate of spit growth by reducing the shoreline angle at the spit entrance (Ashton et al., 2016). Rapid headland erosion forces the fulcrum point to travel more rapidly along the trajectory determined by the wave climate, which is how faster eroding headlands grow longer-necked spits (Ashton et al., 2016). In response, the arc length of the spit end adjusts to the migration rate of the

fulcrum point which, in this case, is to become smaller. A smaller arc length results in more rapid progradation (Ashton et al., 2016). Rapid erosion of the headland also leads to a shallow spit neck angle which significantly reduces sediment input and leads to the conclusion that more rapid spit extension can occur with a decreased sediment input rate (Ashton et al., 2016). While wave climate and basin depth contribute to the influence of spit shape and evolution, models suggest the connection between the spit end and the eroding headland is the most important control on spit shape since the headland controls the difference between sediment input and the maximum in longshore transport (Komar, 1971) determined by wave climate (Ashton and Murray, 2006a; Ashton et al., 2016). Jiménez and Sánchez-Arcilla (2004) suggests, as part of a computer modelling study of spit evolution, that longshore sediment transport is the primary control on decadal-scale shoreline change.

It is hypothesized that 1) barrier spit evolution is episodic and 2) storm activity is a significant external control on barrier spit growth. This research focuses on utilizing GPR and OSL to test these hypotheses by exploring the evolution of the barrier spit complex located in Cape Henlopen, Delaware, USA (Figure 1). The GPR is used to examine the internal architecture of the Cape Henlopen spit features. The OSL is used to age date the relict recurved spits and compare those ages to North Atlantic storm records. A major goal of the research is to obtain enough evidence to argue the control of spit evolution. The general geology of Cape Henlopen has been extensively researched, providing ample data to compare with the data collected during this study. Cape Henlopen State Park has road and trail access to a large portion of the spit complex features used for sample and data collection. Cape Henlopen is also an area with a

comprehensive late Holocene storm record that can be compared with storm records of

other locations throughout the North Atlantic basin.

## 2    Study Area

Cape Henlopen (Figures 1 and 2) is located on the east coast of Delaware where the Atlantic Ocean meets the southernmost portion of the Delaware Bay. Ramsey (1999a) produced a cross section (Figure 3) depicting the three stratigraphic formations associated with this project's study area: the Beaverdam Formation, the Omar Formation, and the Holocene deposits. The Beaverdam Formation is the oldest, ranging from Late
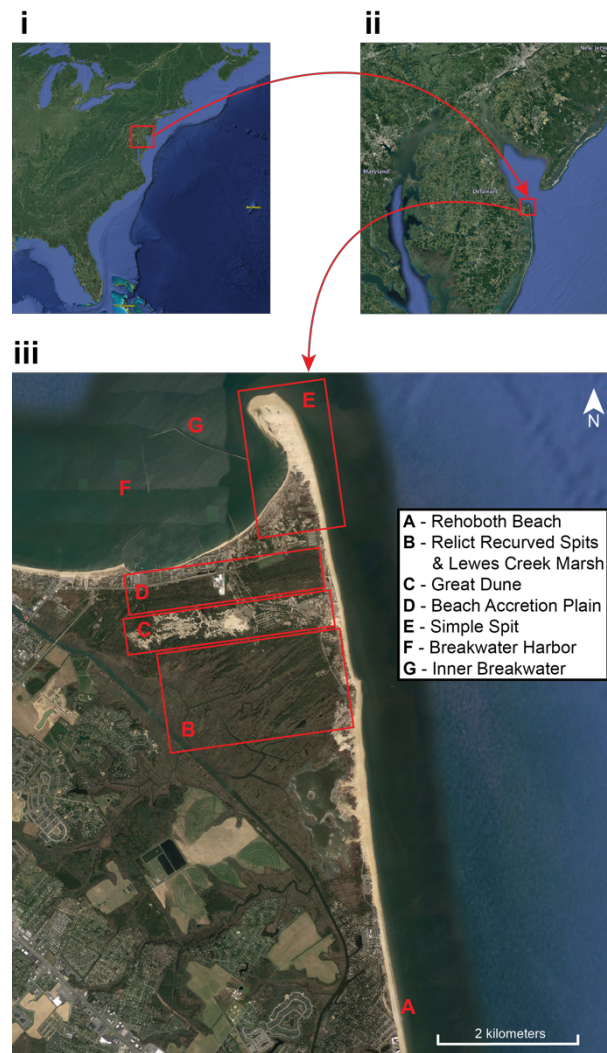


*Figure 1. (i) Satellite image of the eastern United States. (ii) Satellite image of Delaware, highlighting Cape Henlopen on the southern corner of the Delaware Bay and Atlantic Ocean. (iii) Satellite image of Cape Henlopen depicting notable physical features.*

Miocene to Late Pliocene in age and composed of fine to coarse sand with interbedded
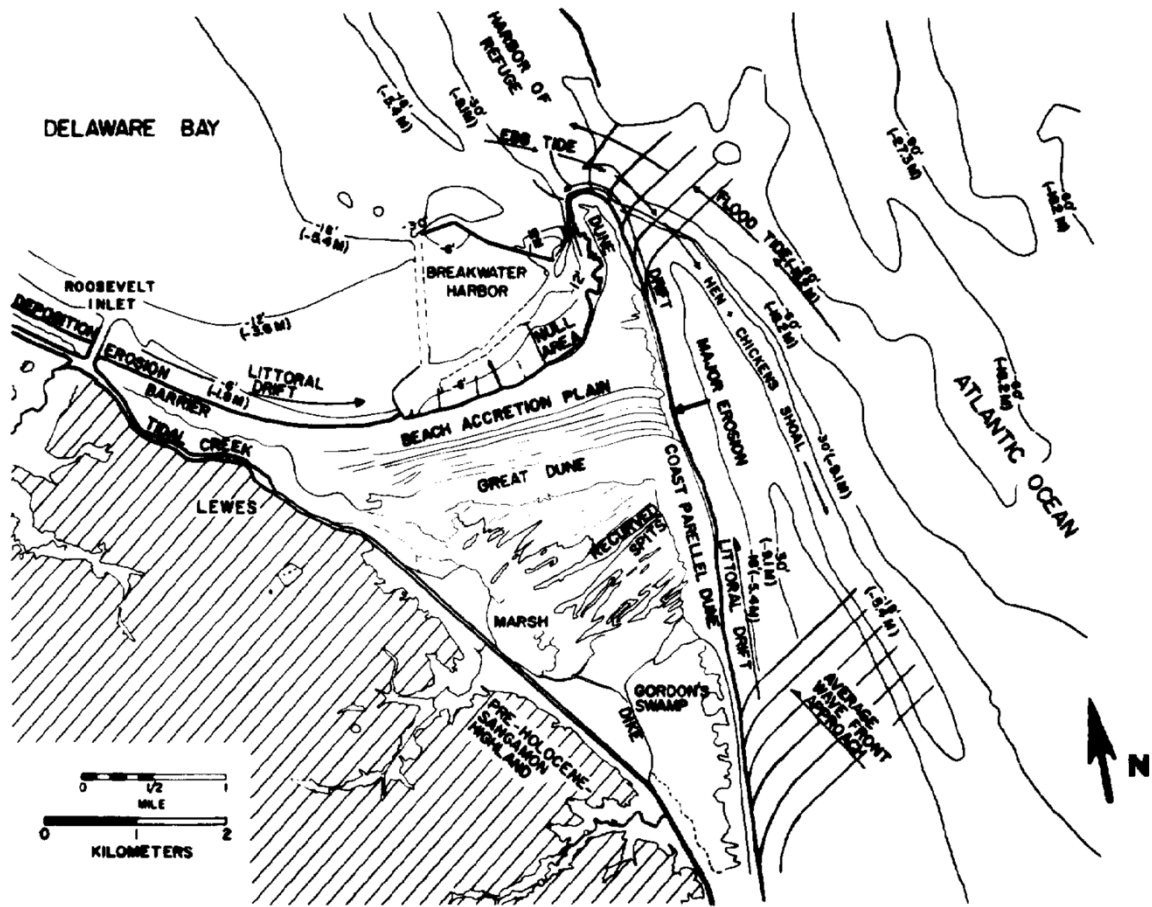
*Figure 2. Diagram showing the geomorphic elements of the Cape Henlopen spit complex and some of the processes that modify the area. From Kraft et al. (1978).*

fine silty sand. The sediments of the Beaverdam Formation are interpreted to be of fluvial

and estuarine environments. The Omar Formation is Late Pliocene to Late Pleistocene in

age with a lithology of clayey sand to sandy silt as well as dispersed beds of fine sand.

The Omar Formation sediments are interpreted to have been deposited in lagoonal,

marsh, and spit environments similar to the presently active coastal system. The

unconformity between the Beaverdam and Omar formations is attributed to subaerial

exposure during sea-level lowstands. The youngest unit consists of Holocene age deposits

composed of fine to coarse sand, sandy to clayey silt, and clayey silt beds abundant in

organics. The unconformity between the Omar Formation and the Holocene deposits
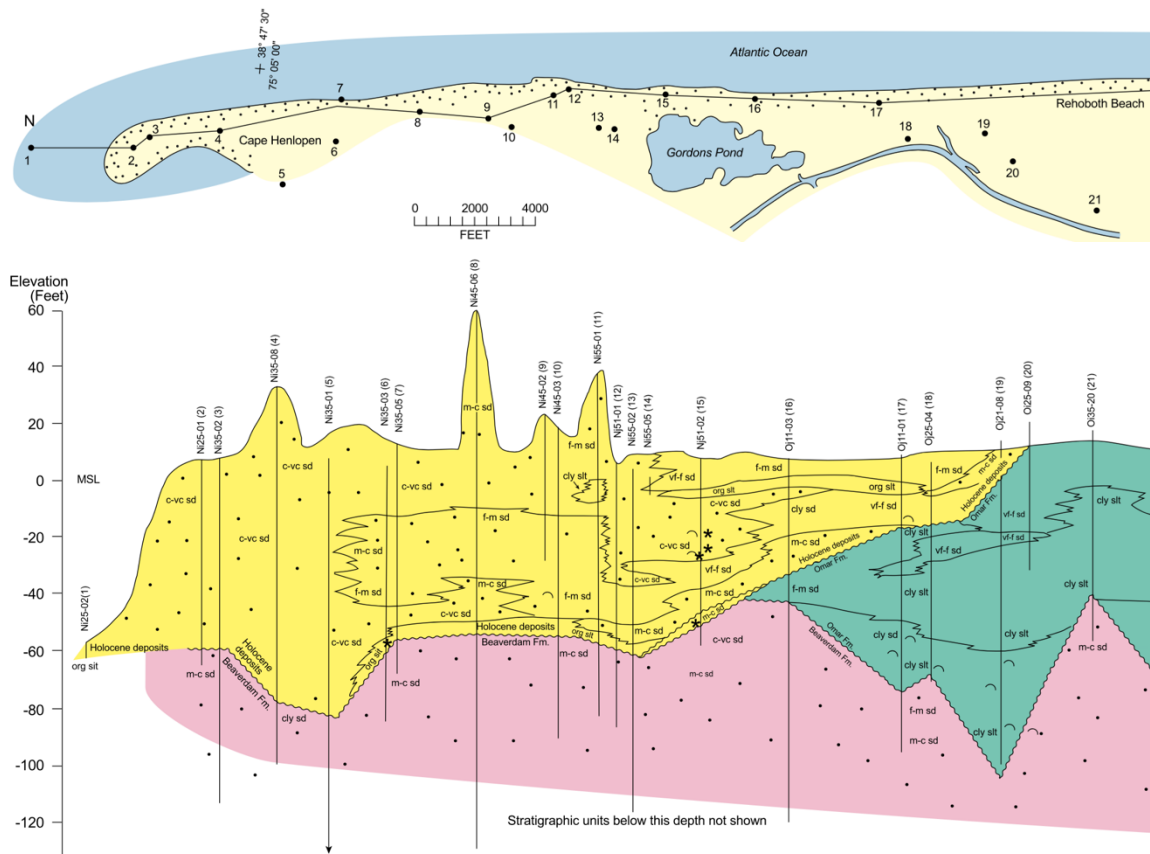
*Figure 3. Geologic cross section showing the general stratigraphy and lithology of Cape Henlopen to Rehoboth Beach, Delaware. Core data for this cross section can be found in Ramsey and Baxter (1996). Figure from Ramsey (1999a).*

corresponds to ravinement surfaces created during marine transgression.

Cape Henlopen contains well-preserved remnants of a millennial-scale northward-growing spit that evolved from a recurved spit complex, to a cuspate spit, to the present-day simple spit (Figure 1). The Cape Henlopen spit system is fed by the shallow marine shelf in the nearshore area and by the erosion of the Pleistocene headlands located to the south around Rehoboth Beach; however, the ultimate source of sand is still unknown (Kraft, 1971; Kraft and Hiller, 1987). The eroded sands are transported northward via longshore drift. As the transported sands reach the tip of the spit system, they encounter the southern mouth of the Delaware Bay. However, there is a net loss in sand unaccounted

for by the rapid advance of Cape Henlopen. Kraft (1971) believes this sand is winnowed out at the tip of the spit and caught in an ebb tidal process that transports the sand seaward onto the Hen and Chickens Shoal, which is a large ebb-tide shoal off the Atlantic Coast of Cape Henlopen. In baymouth barrier washover features and tidal deltas as well as large washover features and high dunes to the south of Cape Henlopen, significant portions of sand from littoral transport are trapped (Kraft, 1971). Kraft (1971) believes sand deposited on the beach from offshore may be derived from a storm-expanded offshore bar.

The tip of Cape Henlopen experiences intense ebb and flood tides. As flood tides enter Delaware Bay, they form gyres due to the Coriolis effect and exit back around the Cape tip with the ebb tide (Kraft et al., 1978). A result of the flood and ebb tides are littoral currents generated in Delaware Bay that flow south and east along Delaware's coast, through Breakwater Harbor, and out to the Atlantic Ocean (Maurmeyer, 1974). Breakwater Harbor (Figure 1) is located in the Delaware Bay north of Lewes Beach and west of the simple spit. Breakwater Harbor is aptly named as it includes what is known as the inner breakwater. The inner breakwater was constructed in 1829-1831 and significantly affects the hydrological and sedimentological processes around Cape Henlopen which will be discussed in further detail along with the geomorphological features of Cape Henlopen.

## 2.1   Relict Recurved Spits

The southernmost geomorphologic feature of the study area is a range of relict recurved spits (Figure 1). According to archaeological evidence and radiocarbon dates the oldest, southernmost of the recurved spits formed around 2.5 ka and the youngest, northernmost of the recurved spits formed around 0.5 ka (Kraft and Hiller, 1987). Initially,

the recurved spit system was located a few kilometers to the southeast of the present-day simple spit and began growing upward and to the northwest with rising sea levels (Kraft and Hiller, 1987). As the recurved spits progressed landward, they created a lagoon off of the Delaware Bay. The lagoon eventually silted in as the youngest recurved spits fused with the mainland between approximately 0.5 ka and 0.4 ka (Kraft et al., 1978). The result of this was the creation of the Lewes Creek Marsh which now encases the relict recurved spits.

## 2.2    Beach Accretion Plain

Northward, towards the coast of Breakwater Harbor in the beach accretion plain (Figure 1) is a series of progradational beach ridges trending parallel to the Breakwater Harbor coast and perpendicular to the Atlantic coast. These beach ridges advanced northward as the Breakwater Harbor coast prograded due to opposing littoral currents. Opposition of the littoral currents is a function of waves refracting south and west around the tip of Cape Henlopen and tidal gyres generating currents flowing south and east along the Delaware Bay coast (Maurmeyer, 1974). This results in the creation of a "null area" in the harbor which induces major sediment deposition (Maurmeyer, 1974). The beach accretion plain was created during the spit system's transition from a recurved spit complex to a cuspate spit around 0.5 ka. Since the construction of Fort Miles in 1941 much of the beach accretion plain has been disturbed by human development (Kraft and Hiller, 1987).

## 2.3    Simple Spit

The northernmost portion of the cape is characterized by a simple spit (Figure 1) being fed with sediments from the Atlantic coast transported via littoral drift to the south.

The spit is characterized by an accretionary tip, and active dune field, tidal flats and swash bars on the Breakwater Harbor coast, and a beach-berm system on the Atlantic coast (Maurmeyer, 1974). Between 1845 and 1997 the simple spit had been prograding northward and slightly westward at a rate of approximately 10 m/yr with an erosion rate of approximately 2.7 m/yr along its Atlantic beaches (Galgano Jr., 2008). The simple spit is composed of Holocene sands and gravels which extend from the berm and tidal flat surface to the upper boundary of the Beaverdam Formation estuarine sediments (Kraft and Hiller, 1987).

## 2.4   The "Great Dune"

Between and atop the beach accretion plain and the relict recurved spits is what is known as the Great Dune (Figure 1). The Great Dune is an east-west trending, roughly 25-meter above sea level, 3- to 4-kilometer-long dune that is subparallel to the Breakwater Harbor coast and perpendicular to the Atlantic coast (Kraft et al., 1978). The Great Dune is regarded as an anomalous feature in the Cape Henlopen complex. Kraft and Hiller (1987) state that the possible cause of the dune's formation was deforestation around Cape Henlopen during the construction of the inner breakwater which permitted northerly aeolian processes to transport beach sediments and generate the dune. The Great Dune migrates south-southeast at an average rate of 1.7 m/yr and is beginning to bury the youngest of the relict recurved spits (Kraft and Hiller, 1987).

## 3   Literature Review

## 3.1   Sediment Grain-Size Analysis

Sediment grain-size analysis is a common analytical geologic procedure used to

characterize the physical properties of sediment. By determining a sediment sample's grain-size distribution, the sorting, mean, skewness, and kurtosis of the sediment sample may be calculated. These properties are important for determining the classification of sediment, the process(es) sediment endured during transport, and the depositional environment of the sediment. The traditional way to measure sediment grain size and distribution is by the use of sieves. This method involves stacking sieve pans, each equipped with a particular mesh size, atop of one another so that the larger mesh pans are above the smaller mesh pans. As a sediment sample is placed in the uppermost pan, the larger sediments are trapped in the larger mesh pans and the smaller sediments drop to, and are trapped by, the smaller mesh pans. The result is a fractionation of the sediment sample based on the particular screen sizes used in the stack of sieves.

However, with the rise of computer technology, there now exists fully computerized grain-size analyzers that utilize light diffraction patterns of sediment samples passing through a device's laser beam. With this method, grain-size distribution is computed by measuring the angular variation in scattered light intensity as a laser beam travels through the sediment sample (Malvern Ltd., 2015). Since large sediment grains scatter light at small angles relative to an incident light ray and small grains scatter light at large angles relative to an incident light ray, the Fraunhofer diffraction theory of light scattering is used to calculate the size of particles based on the detected light diffraction patterns (Malvern Ltd., 2015).

### 3.1.1 Cape Henlopen Sediments

Kraft et al. (1978) performed extensive grain-size analysis on sediments from Cape Henlopen. By using standard sieve series screens they were able to determine the

14

general sediment particle sizes of each major environment in Cape Henlopen. The beach and nearshore environments, including spit deposits, are composed of medium to coarse sands with some gravels. Lewes Creek Marsh is composed mostly of organic muds. Estuarine sediments vary greatly from interlaminated sands to muds containing shells and lithic pebbles, all of which being heavily disturbed by burrowing marine organisms.

## 3.2    Ground Penetrating Radar (GPR)

GPR provides a non-invasive method of imaging the shallow subsurface of Earth. Short pulses of high-frequency electromagnetic energy are transmitted from an antenna into the subsurface. As an energy pulse encounters boundaries between different lithologies within the subsurface a portion of the energy pulse is reflected back to the antenna's receiver, where it is recorded. The time between the transmission and reception of an energy pulse is measured in nanoseconds and known as the two-way traveltime (TWT) (Neal, 2004). The strength of the energy reflection is approximately proportional to the contrast in dielectric properties between different types of material, as may be found at a lithologic boundary (Davis and Annan, 1989).

A 100 or 200 MHz antenna is commonly used for surveying coastal environments due to their balance of suitable penetration depth and resolution. The TWT recorded in nanoseconds by the antenna, are typically converted to depth. Radar facies, which are the visible differences in a GPR profile that result from the characteristics of reflection patterns produced by sedimentary layers, are used to interpret stratigraphy (Van Overmeeren, 1998). Some factors that influence the visible reflection patterns in a GPR profile include: reflection amplitude, reflection continuity, reflection configuration, dominant frequencies, abundance of reflections, and degree of penetration (Van Overmeeren, 1998). The radar

15

stratigraphy and depositional environments can then be interpreted from the radar facies by correlating the reflection patterns with patterns of specific sedimentary environments as well as ground truthing from sediment core data (Van Overmeeren, 1998).

There have been several GPR studies conducted in the Cape Henlopen area, such as the investigations performed by Daly et al. (2002) and Chadwick and Madsen (2000). These two investigations yielded similarly defined sedimentary facies: the spit platform facies and the overlying spit beach and dune facies.

### 3.2.1 Cape Henlopen Archaeological GPR Study

Chadwick and Madsen (2000) conducted an archaeological study using GPR to survey shell midden deposits. The shell midden imaged in this study is located on the distal end of a central relict recurved spit tip. A 400 V transmitter and 100 MHz antenna were used to perform the survey. A velocity of 0.07 m/ns for the GPR waves was assumed to convert the TWT to depth. GPR reflection depths ranged from tens of centimeters up to approximately 7 meters. The survey displayed four distinguishable GPR facies. Chadwick and Madsen (2000) interpreted these GPR facies as spit platform, spit, dune, and shell midden deposits (Figure 4). The lowermost GPR facies, interpreted to be spit platform deposits, is characterized by poorly to moderately developed, steeply dipping reflections bounded on the top and bottom by nearly horizontal reflections and occurs between 3-6 m depth. The next GPR facies occurring between depths of 1.2-3 m depth, interpreted to be spit beach deposits, is characterized by well developed, shallower dipping reflections bounded on the bottom by the upper boundary of the spit platform facies. The upper boundary of the spit facies is only sometimes well defined by a nearly horizontal reflection. Occurring between approximately 1.5 m depth and the ground

surface is the GPR facies interpreted to be dune deposits characterized by discontinuous, horizontal to shallow dipping reflections with cross-bedding present as well. It is noted that only one of the profiles collected displayed a well-defined bottom boundary of the dune facies. Within the uppermost GPR facies are anomalous concave-upward reflections that are circular in horizontal distribution. This GPR facies is interpreted to be shell midden deposits.
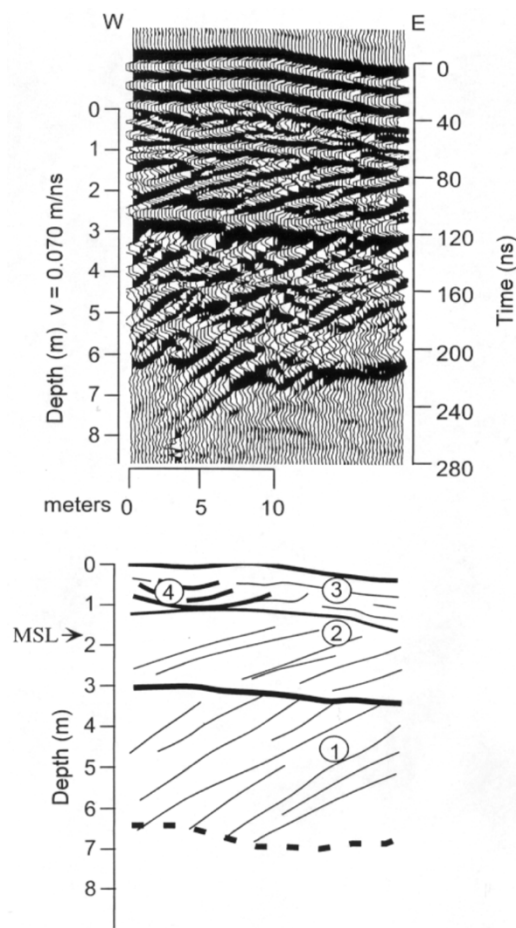


*Figure 4. A west-east GPR profile with interpreted cross-section below. Interpretations based on GPR reflections are: (1) Spit Platform, (2) Spit, (3) Dune, (4) Shell Midden. From Chadwick and Madsen (2002).*

17

### 3.2.2 Cape Henlopen Geological GPR Study

Daly et al. (2002) took a more in-depth geological approach to surveying Cape Henlopen with GPR. Several transects in three different areas of Cape Henlopen were surveyed with profiles both parallel and perpendicular to the linear spit deposits (Figure 5). A 100 MHz antenna was used. Daly et al. (2002) identifies four radar facies throughout the relict recurved spits, beach accretion plain, and modern simple spit areas: oblique facies, parallel facies, hummocky facies, and reflection-free facies. The oblique facies, subdivided into tangential-oblique and sigmoidal-oblique facies, are present in GPR profiles collected perpendicular to spit or ridge axes. Similar to the spit platform and spit facies reflections in the Chadwick and Madsen (2000) study, the oblique radar facies in this study are characterized by downlap and toplap termination onto a high-amplitude, continuous, near horizontal reflection surface. Daly et al. (2002) interpret the tangential-oblique facies as progradational beachface and dune sediments. The sigmoidal-oblique facies are interpreted as progradational spit-platform sediments. The parallel and hummocky facies are present in GPR profiles collected parallel to spit or ridge axes. The parallel reflections are high-amplitude, continuous, horizontal to subhorizontal, and interpreted as aggrading spit sands and gravels.

These parallel reflections can be matched with oblique radar facies in profiles perpendicular to spit or ridge axes. The hummocky facies are more sporadic, only appearing as occasional mound-shaped structures. Hummocky facies can be found adjacent to parallel facies and is interpreted as internal bedding of dunes. Reflection-free facies are associated with GPR signal attenuation caused by saltwater intrusion or brackish porewaters retained in estuarine sediments beneath spit deposits.
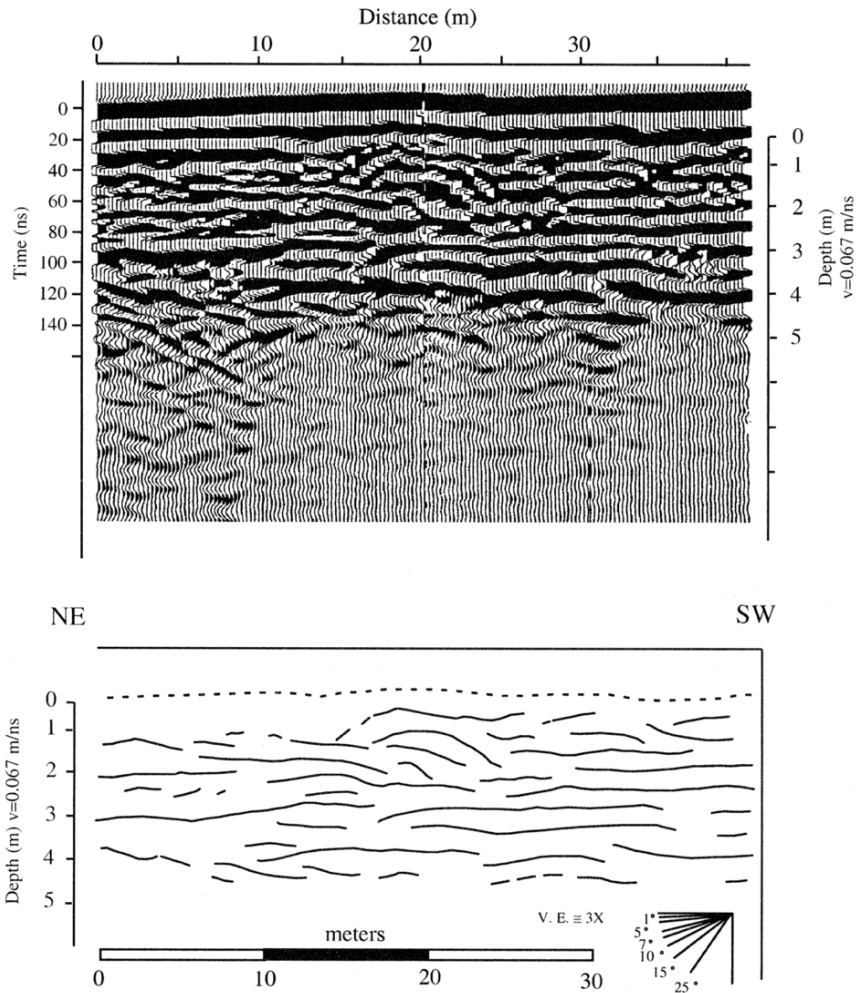
*Figure 5. 100MHz GPR data and line drawing interpretation of a profile collected parallel to the axis of a recurved spit in Cape Henlopen. TWT is in nanoseconds and depth is in meters (not relative to mean sea level). In the interpretation, the dashed line indicates the approximate ground surface. From Daly, McGreary, and Krantz (2002).*

### 3.2.3   Sylt Spit GPR Study

The overall sedimentary facies patterns documented of the Cape Henlopen spit complex are not unique to the Cape Henlopen location. Spit systems in other areas of the world exhibit similar subsurface facies patterns. Sylt is an island in the Wadden Sea off the coast of northern Germany that contains a Holocene spit on its southern end. Tillman and Wunderlich (2011) performed a GPR investigation on southern Sylt using a 200 MHz antenna to reveal an erosional surface overlain by prograding barrier spit platform and

19

beachface facies capped by aeolian dune facies (Figure 6). The erosional surface on which the progradational spit sediments lie is an unconformity located approximately 7 m below the ground surface. This erosional surface is thought to be caused by intense storm surges. The prograding barrier spit sequence that overlies the erosional surface is characterized by continuous, high amplitude, sigmoidal to tangential oblique reflections. These reflections observed by Tillman and Wunderlich (2011) closely resemble those found in the Daly et al. (2002) Cape Henlopen investigation which were interpreted as progradational spit-platform and progradational beachface deposits. Near the upper boundary of the prograding barrier spit sequence (approximately 2.5 m below the ground surface) are continuous, medium amplitude, gently dipping to horizontal reflections. These reflections are interpreted by Tillman and Wunderlich (2011) to be of spit beach deposits which also resemble the spit beach reflections in the Cape Henlopen GPR surveys. From the upper boundary of the prograding barrier spit sequence to the ground surface are high amplitude, moderately continuous, highly dipping reflections interpreted by Tillman and Wunderlich (2011) to be cross-bedded aeolian dune sediments. This type of aeolian dune cap is also commonly observed in Cape Henlopen GPR profiles.

Additionally, all of the radar facies observed in the aforementioned GPR investigations are comparable to the atlas of radar facies created by Van Overmeeren (1998) which presents examples of GPR profiles with their respected interpretations and written description of characteristics for various sedimentary environments.
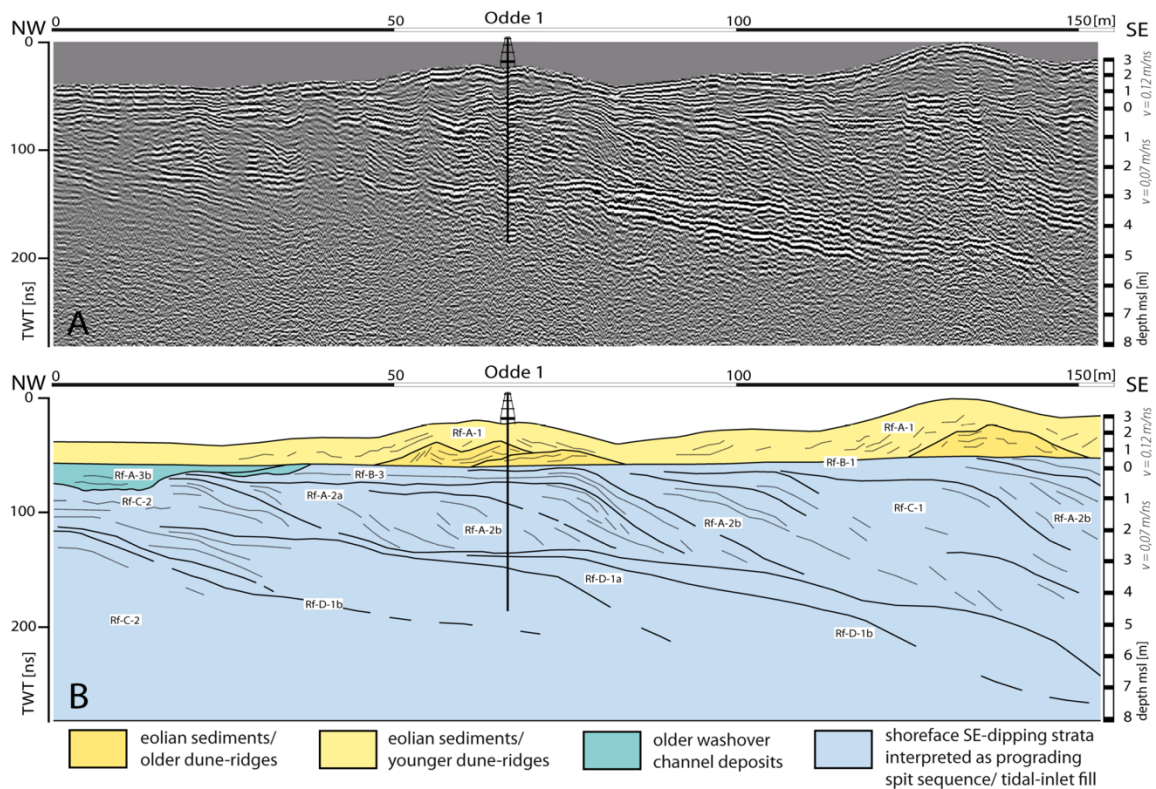
*Figure 6. Northwest-southeast GPR profile roughly parallel to the axis of the southern Sylt spit. A: Profile of GPR data with TWT in ns on the left axis and depth relative to mean sea level in meters on the right axis. B: Interpretation and legend of the GPR profile in A. Solid lines are erosion and bounding surfaces and dashed lines display internal structures. From Tillmann and Wunderlich (2011).*

## 3.3 Optically Stimulated Luminescence (OSL)

OSL dating provides a means of calculating the elapsed time between measurement and a mineral grain's last exposure to daylight, or last heating to a few hundred degrees Celsius (Huntley et al., 1985; Murray and Roberts, 1997; Aitken, 1998; Lang et al., 2003; Rodnight et al., 2005; Preusser et al., 2008; Rhodes, 2011; Shen and Mauz, 2012). Quartz and feldspar are the most commonly used minerals for OSL operations. The process begins as, for instance, a quartz grain is bleached by daylight. Bleaching is the removal of trapped charge (Figures 7 and 8) within a mineral grain by exposure to light (Rhodes, 2011). As the quartz grain is buried and removed from the light or heat source, it accumulates trapped charge (Figures 7 and 8). The environment

21
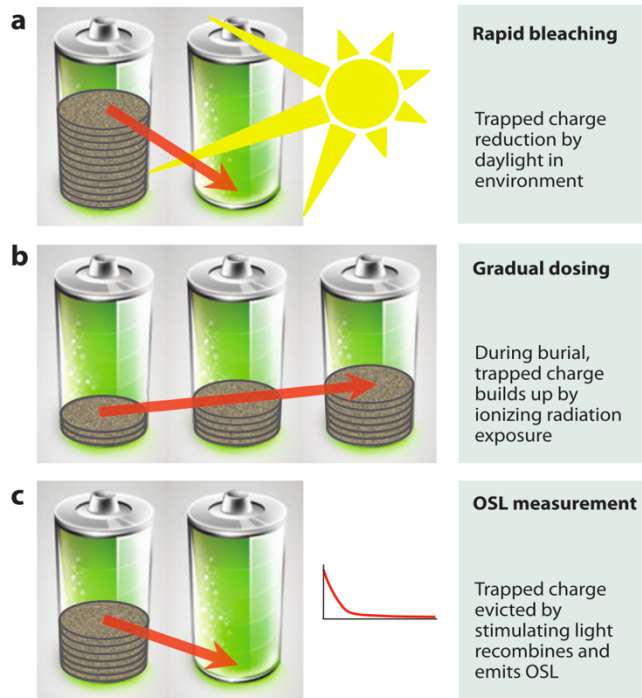
*Figure 7. Rechargeable battery analogy to bleaching and ionizing radiation of grains. (a) Trapped charge is released by daylight over periods of seconds to minutes. (b) Natural radiation sources in burial environment builds trapped charge at defects within grains. (c) Light stimulation in a laboratory releases trapped charge which recombines emitting a luminescence signal, resulting in an OSL decay curve (shown). From Rhodes (2011).*

contains natural radiation from the decay of radioactive isotopes of uranium (U) and thorium (Th) decay chains, potassium ($^{40}$K), and from cosmic rays. As electrons within the crystal are ionized from the valence band to the conduction band by radiation, a portion of them subsequently become trapped in the forbidden gap between valence and conduction bands (Rhodes, 2011). The traps can be at different depths below the conduction band.

Deeper electron traps are more stable than shallow traps. The quartz grain accumulates trapped energy from environmental radioactive decay over time until it experiences another bleaching event. Some minerals, such as quartz and feldspar, release the trapped energy in the form of light called luminescence (Huntley et al., 1985; Duller, 2008). Luminescence occurs as the trapped electrons are released and recombine with holes at
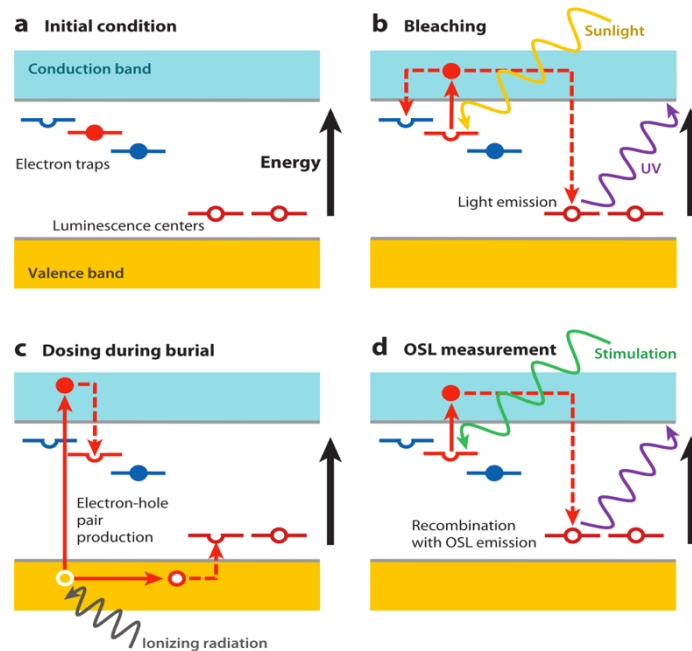
*Figure 8. Band gap energy model of OSL. Red shapes are OSL electron traps and blue shapes are thermoluminescence traps. (a) Thermal eviction at ambient temperature keep low thermal stability traps close to the conduction band empty, but other traps are filled. Luminescence centers are available. (b) Exposure to light evicts electrons in OSL traps. The electrons may become trapped in other available sites or recombine at luminescence centers. All OSL traps are emptied after sufficient light exposure. (c) During burial, environmental ionizing radiation increases OSL trap population. (d) Laboratory light stimulation evicts electrons from OSL traps which recombine at luminescence centers to produce a luminescence signal. Figure from Rhodes (2011).*

luminescence centers which results in the emission of light photons (Huntley et al., 1985; Duller, 2008). This luminescence can be observed in a laboratory and used to estimate the amount of time passed since the grain's last bleaching when used in conjunction with the amount of radiation absorbed per year, called dose rate. Gray (Gy), or J/kg, is the SI unit of radiation dose and dose rate is measured in Gy/year (Rhodes, 2011).

### 3.3.1 Preheating and Stimulation Light Sources

Before making any OSL measurements, an aliquot must be preheated to empty the undesired, unstable shallow electron traps but retain the deep stable traps desired for dating measurements (Aitken, 1998; Duller, 2008). Preheat temperatures are typically around 160-280°C (Murray and Wintle, 2003). Figure 9 displays a typical OSL detection system. A suitable stimulation light must also be used for measurements. The light must

23

be restricted to a narrow wavelength range so that it can be filtered out before reaching

the photomultiplier tube (Duller, 2008). Blue and green light emitting diodes (LEDs) are

typically used as stimulation lights because they can successfully generate an OSL signal

from quartz, they have a different wavelength than the luminescence signal, and they are

able to be filtered out (Duller, 2008). Sometimes, infrared LEDs are used to evaluate how

much feldspar is present in an aliquot of quartz grains. Infrared stimulated luminescence
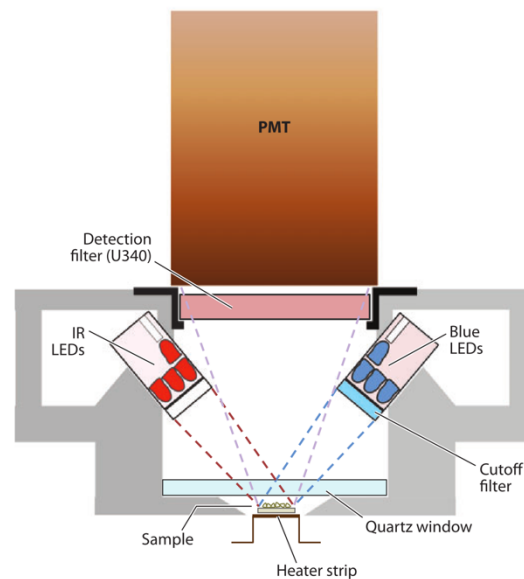


*Figure 9. Schematic of a typical OSL/IRSL detection system based on the Risø TL-DA-20. The sample is placed on a heater plate and illuminated by stimulation wavelengths from blue, green, or IR LEDs. Luminescence signal is detected through a U340 filter by the photomultiplier tube (PMT). Figure from Rhodes (2011).*

(IRSL) is not observed from quartz at room temperature; however, feldspar does provide

IRSL signal (Duller, 2008).

### 3.3.2    Measurement of Equivalent Dose

The single aliquot regenerative dose (SAR) protocol is the most commonly used

optical dating procedure to measure radiation dose absorbed in a mineral (Figure 10). The

SAR protocol was primarily developed by Murray and Wintle (2000, 2003) which

consists of measuring both the OSL from the unknown dose absorbed since the last

bleaching and multiple OSL from known laboratory doses using a single aliquot. There are multiple cycles in the SAR method. Before the first cycle the aliquot is preheated to around 160-280°C (Murray and Wintle, 2003). The first cycle is the measurement of an aliquot's luminescence signal (L) of radiation absorbed from the natural environment ($L_N$) (Duller, 2008). The aliquot is then given a fixed artificial test dose ($T_x$). The aliquot is then preheated, and the signal is measured. After the test dose signal is measured the aliquot is irradiated with a regenerative dose in the second cycle. The aliquot, now with a regenerative dose ($L_x$), is preheated and measured just as the $L_N$ signal was measured in the first cycle. This process is repeated for multiple regenerative doses. Each regenerative dose ($L_x$), including natural and zero dose, luminescence signal is normalized by the subsequent test dose ($T_x$) luminescence signal with the ratio $L_x/T_x$ (Murray and Wintle, 2003; Preusser et al., 2008). This ratio gives a sensitivity-corrected luminescence signal for each dose and is used to create a dose response curve (Murray and Wintle, 2003; Preusser et al., 2008). The equivalent dose ($D_e$), which is the amount of laboratory radiation equivalent to the amount of natural radiation received during burial, can be determined using a dose response curve (Duller, 2008).
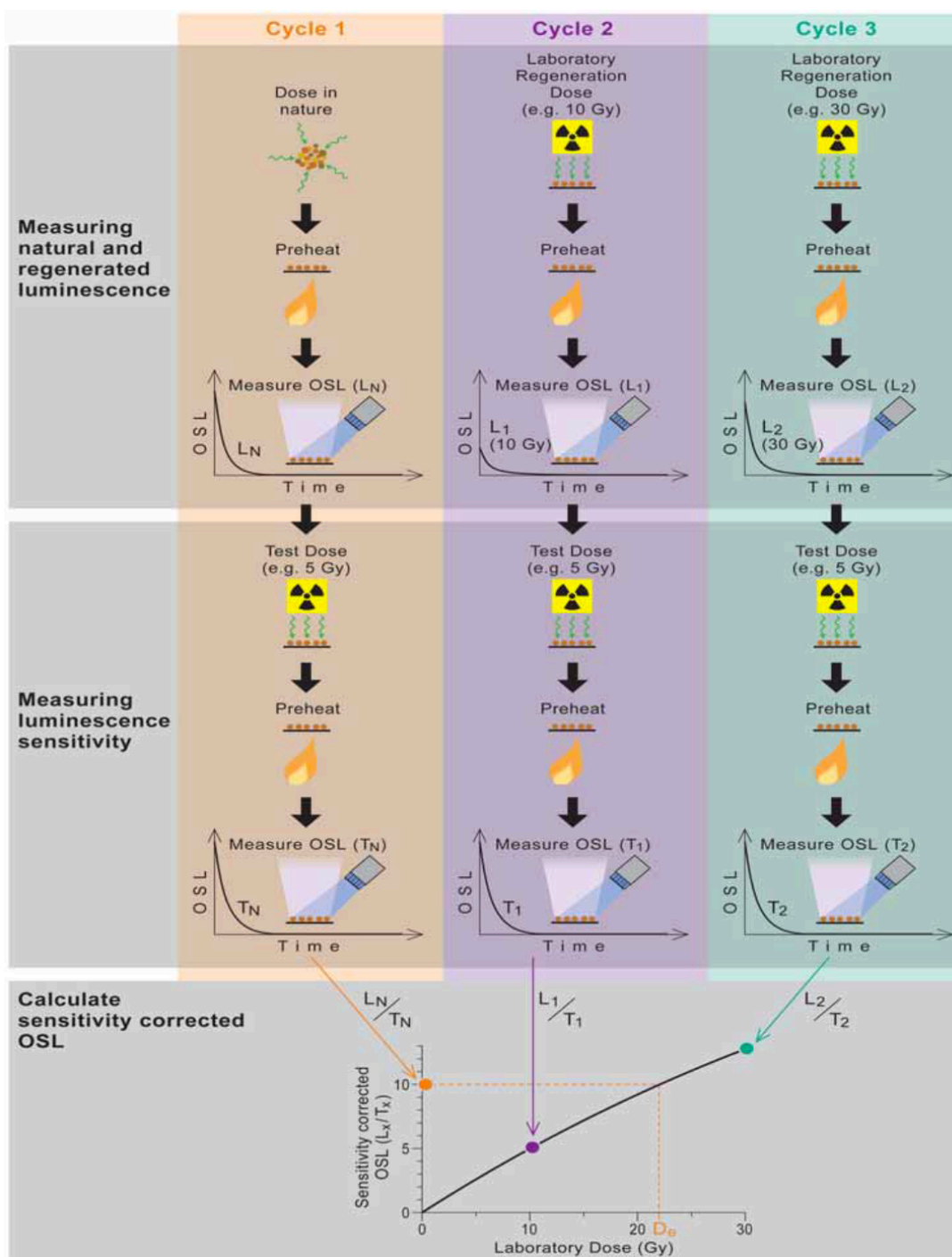
*Figure 10. SAR procedure applied to quartz. The sample is administered numerous laboratory doses (regenerative doses) of different radiation amounts (10Gy, 30Gy, etc) which are measured ($L_1$, $L_2$, etc). After each measurement the luminescence sensitivity is tested by applying a fixed dose (here 5Gy) and measuring the result ($T_1$, $T_2$, etc). Sensitivity is corrected for by the ratio $L_x/T_x$. By plotting the $L_x/T_x$ values the $D_e$ (here 22Gy) can be determined for that aliquot when the measurements of the natural signal ($L_N/T_N$) are plotted. Figure from Duller (2008).*

### 3.3.3 Recycling Ratio Test

The final regenerative dose given to an aliquot is used to perform a recycling ratio test, which evaluates the sensitivity correction of each aliquot. Sensitivity is the amount of luminescence an aliquot emits per unit of radiation dose, which changes based on the burial conditions and the laboratory procedures used. The recycling ratio test is used to compensate for such changes. The final dose is identical to the first regenerative dose. The recycling test is in the form of a ratio; therefore, the recycling ratio is of the final sensitivity-corrected luminescence signal (e.g. $L_7/T_7$) to that of a previous dose of the same value (e.g. $L_2/T_2$) (Murray and Wintle, 2000; Rhodes, 2011). Ideally, the recycling ratio value should be 1.0, but a value between 0.9 and 1.1 is acceptable (Murray and Wintle, 2003).

### 3.3.4 Thermal Transfer

In OSL, thermal transfer is the movement of charge into luminescence traps from other traps (Rhodes, 2011; Shen et al., 2011). Recuperation is when charge is transferred to less stable traps from luminescence traps and then back to the luminescence trap during preheating, which results in unwanted signal during the preheating stage (Rhodes, 2011; Preusser et al., 2008). Recuperation and thermal transfer can be tested. A recuperation test is performed by giving an aliquot a zero-regenerative dose followed by a test dose of the same value as the previous SAR cycles. For $L_0/T_0$ the value should, ideally, be 0.0; however, a value of 5% or less of the $L_N/T_N$ value is deemed acceptable (Murray and Wintle, 2000; Preusser et al., 2008).

### 3.3.5 Dose Recovery Test

A dose recovery test is used to prove that a known, laboratory-administered dose

can be matched by the SAR measurement procedure (Preusser et al., 2008). The test

begins by zeroing the signal of an aliquot and then irradiating it with a known dose. A

dose similar to the $D_e$ value of the aliquot is usually administered (Duller, 2008) (Figure

11). The SAR procedure is then performed. The calculated dose should equal the

administered dose. If the calculated dose does not match the laboratory dose then it is
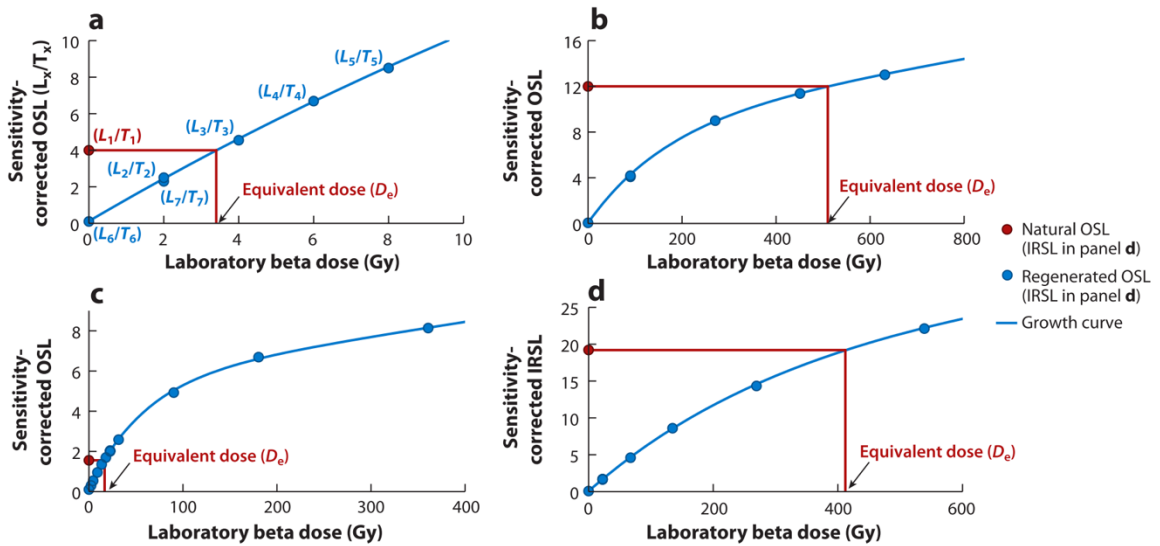


*Figure 11. OSL and IRSL growth curves for determining $D_e$. (a) Typical curve produced with SAR protocol comprising seven steps. Natural and regenerative dose OSL ($L_x$) is corrected by the OSL response to the test dose ($T_x$). The red ($L_1/T_1$) is the natural OSL and the blue ($L_2/T_2$, $L_3/T_3$, etc) are the regenerative dose OSL measurements for that aliquot. (b) Result of measuring the response of an older quartz aliquot, which is approaching saturation. (c) Result of measuring the response of a quartz aliquot from a late Pleistocene fluvial deposit. (d) IRSL of feldspar from an older sample. Note that curve is less pronounced than the quartz curve in panel c due to the minerals' different saturation characteristics. Figure from Rhodes (2011).*

improbable that the aliquot's calculated $D_e$ value will be correct (Duller, 2008).

### 3.3.6   Variations in $D_e$

There is variation in $D_e$ values for different aliquots of a sample, termed

overdispersion. Overdispersion is the amount of $D_e$ variation that cannot be accounted for

by known laboratory sources. Significant variation is indicative of diverse dose values for

individual grains that constitute the aliquots (Rhodes, 2011). The fundamental causes of

$D_e$ overdispersion are incomplete bleaching and beta dose heterogeneity. Incomplete

28

bleaching describes when the population of trapped electrons in some grains within a sample was not entirely reset during the natural bleaching event (Duller, 2008). Situations of incomplete bleaching can be dealt with during analysis by various statistical age models. Another possible cause of variation is differences in dose rate in different portions of the sample. This could be caused by different parts of the sample receiving different doses of radiation during burial (Duller, 2008). However, there is the potential for highly radioactive material to be present in certain environments where a sample may be very heterogeneous (Duller, 2008). Postdepositional mixing of grains caused by, for instance, bioturbation or human activity, or errors during sampling could also produce variation in $D_e$ values (Duller, 2008; Rhodes, 2011). Another proposed cause of $D_e$ overdispersion is beta radiation microdosimetric effects. Mayya et al. (2006) suggests microscopic fluctuations in the spatial distribution of feldspar containing $^{40}K$ beta radiation emitters can produce overdispersion. Intrinsic statistical fluctuations occur on the scale of beta particle ranges despite an apparent homogeneous distribution of feldspar in a sample, which results in variations of beta radiation doses to grains (Mayya et al., 2006).

It is important to consider grain and aliquot size in interpreting $D_e$ overdispersion. It is common to use sand-sized grains to create aliquots of around a thousand grains, hundreds of grains, tens of grains, or a single grain (Duller, 2008). The more grains composing an aliquot the less visible variation in $D_e$. This is because the averages of aliquots with hundreds or thousands of grains essentially mask the variations; therefore, if such aliquots are suspected of having been subject to incomplete bleaching or mixing then measurements using fewer grains may be required (Duller, 2008).

### 3.3.7 Dose Rate

Dose rate is the amount of radiation a sample received per year. The dose rate is assumed to be constant through the elapsed time of burial. There is a total of four types of radiation that could affect a sample: alpha particles ($\alpha$), beta particles ($\beta$), gamma rays ($\gamma$), and cosmic rays (Duller, 2008). Alpha, beta, and gamma radiation are mainly generated by the decay of natural radioactive isotopes of uranium (U), thorium (Th), and potassium (K). The radioactive potassium isotope, $^{40}K$, decays to the stable calcium ($^{40}Ca$) or argon ($^{40}Ar$) isotopes through emission of beta and gamma radiation (Duller, 2008). The radioactive uranium and thorium isotopes present a much more intricate decay series. Unlike potassium, uranium and thorium decay to other radioactive isotopes through emission of alpha, beta, and gamma radiation before becoming stable (Duller, 2008). Cosmic rays are a form of high energy electromagnetic radiation. Only a portion of cosmic rays reach the surface of Earth due to atmospheric shielding. The portion that does reach the surface attenuates rapidly within the uppermost meter of sediment. Each type of radiation travels a different distance through sediment. Alpha particles travel about a few hundredths of a millimeter, beta particles travel a couple of millimeters, and gamma rays travel up to 0.3 meters (Duller, 2008).

There are three established ways to measure dose rate: 1) by using dosimeters directly in the sampling site; 2) by using radiation counting devices to measure alpha, beta, and gamma radiation; and 3) by analyzing dose rate relevant nuclide concentration and activity (Preusser et al., 2008). Laboratory measurement of radioactive elements usually involves equipment such as inductively coupled plasma mass spectrometers (ICP-MS) or neutron activation analysis (NAA) and may require samples to be dissolved in acids

30

(Preusser et al., 2008). After concentrations of the radioactive elements are measured, they are converted to dose rate of each type of radiation which are then added together to obtain the total radiation dose rate. It should be noted that the gamma dose rate can only be accurately measured in a laboratory if the material surrounding the sample is homogeneous 0.3 meters in all directions (Aitken, 1998).

Environmental water content has an effect on a sample's dose rate. The more water present during a sample's burial, the less radiation absorbed by the grains composing the sample (Duller, 2008). This can be accounted for through calculations if the water content during burial can be estimated, which can be done by measuring the saturation water content and measuring the present-day environmental water content (Duller, 2008).

The cosmic ray contribution must also be accounted for. The amount of cosmic ray contribution depends on the latitude, altitude, and depth of a sample beneath the surface (Prescott and Hutton, 1994). Typically, the latitude of a sample is only significant if it is greater than 60°N or S and the altitude of a sample is only significant if it is more than 500 meters above sea level (Duller, 2008). The depth at which the sample lies beneath the surface generally has the greatest impact on cosmic dose rate. If the sampling site is within the mid-latitudes, near sea level, and buried beneath about 0.3 meters of material then the cosmic dose rate will be around 0.2 Gy/ka; if the sample is buried beneath about 10 meters of material the cosmic dose rate will be around 0.07 Gy/ka (Duller, 2008).

### 3.3.8 Age Determination

The age of a sample can be calculated using the following equation: age in years = $D_e$ (Gy) / dose rate (Gy/yr) (Rhodes, 2011). The upper age limit is usually controlled by

luminescence signal saturation (Wintle and Murray, 2006) and dose rate. Signal saturation is achieved when all electron traps become full; therefore, even if there is continuing exposure to radiation the luminescence signal will not increase. The lower age limit is influenced by the amount of incomplete bleaching and the luminescence sensitivity of the minerals composing the sample (Duller, 2008).

Statistical age models can be used when there is significant variation in $D_e$ values, as mentioned in Section 2.3.6. One model is the central age model (Galbraith et al., 1999). The central age model is primarily used for well-bleached samples. It estimates the uncertainty, mean dose, and overdispersion (Rhodes, 2011). For samples subject to incomplete bleaching, which produces skewed dose distributions towards higher $D_e$ values, the minimum age model (MAM) may be used (Galbraith et al., 1999).

### 3.4 Storm History

In order to determine a relationship between spit development and storm activity, a storm history must be compiled. Numerous studies have been performed throughout the North Atlantic basin in efforts to establish detailed storm records based on data obtained using ground penetrating radar, grain size analysis, optically stimulated luminescence and radiocarbon dating, and sediment cores (Jackson et al., 2005; Buynevich et al., 2007; Donnelly and Woodruff, 2007; Sorrel et al., 2009; Sabatier et al., 2012; Toomey et al., 2012; Sorrel et al., 2012; Nikitina et al., 2014; Donnelly et al., 2015; Van Hengstum et al., 2014, 2015). Dates of interpreted storm events are compiled from Delaware, Massachusetts, Maine, Bermuda, Puerto Rico, the Bahamas, Iceland, northwest France, and the northwest Mediterranean. It is apparent that there is coinciding evidence of increased storm activity in the North Atlantic basin from approximately CE 0 to 700

(2.01 – 1.31 ka) and CE 1300 to 1700 (0.71 – 0.31 ka). The ages in this section and the following section refer to CE 2017, the year of OSL measurements for this research.

### 3.4.1 Periods of Increased Storm Activity

Nikitina et al. (2014) conducted a storm history investigation of the Sea Breeze salt marsh in Delaware Bay, New Jersey by gouge coring along seven transects. The oldest salt marsh erosional surface interpreted to be caused by storm activity was dated around CE 240 (1.77 ka) by radiocarbon dating. This age coincides very well with coarse-grained, storm-induced deposits, or event beds, preserved in coastal lakes and marshes in Salt Pond, Massachusetts (Donnelly et al., 2015). Donnelly et al. (2015) used radiocarbon and pollen dating techniques, as well as stratigraphic data to date a period of heightened frequency coarse-grain event bed deposition between CE 240 and 1140 (1.77 and 0.87 ka). Similar aged evidence can be found in Maine. Buynevich et al. (2007) used GPR and OSL in the western Gulf of Maine to date relict scarps linked to severe beach erosion and retreat attributed to storm activity. The oldest scarp is dated at CE 390 (1.62±0.17 ka). There is similarly aged stratigraphic evidence of storm activity found along the Gulf of Mexico, the Netherlands, and southern Portugal (Jelgersma et al., 1995; Liu and Fearn, 2000; Andrade et al., 2004; Buynevich et al., 2007). Europe also shows evidence of a Holocene storm period within this interval. Sorrell et al. (2012) used seismic reflection surveys, vibracores, and radiocarbon dating in the Seine Estuary and Mont-Saint-Michel Bay (MSMB) of northwest France to identify storm deposits. One of the Holocene storm periods dated in this area ranged from CE 50 to 900 (1.96-1.1 ka). In another study, Van Hengstum et al. (2015) used mean grain size data from Walsingham Cavern, Bermuda as proxies from storminess in Bermuda. The results of this study were also compared to grain size data

33

compiled from Iceland, NW France, the NW Mediterranean, Puerto Rico, and the Bahamas (Jackson et al., 2005; Donnelly and Woodruff, 2007; Sorrel et al., 2009, 2012; Sabatier et al., 2012; Van Hengstum et al., 2014; Toomey et al., 2012). In Bermuda, mean grain size data indicates increased storminess from CE 150 to 650 (1.86 to 1.36 ka). In the NW Mediterranean, lagoon washover events were dated between CE 50 to 550 (1.96-1.46 ka). The storm activity data for the NW Mediterranean is correlated to the 1500-year cycle of ice rafted debris deposition and cooling in the North Atlantic region (Sabatier et al., 2009; Van Hengstum et al., 2015). In Iceland, increased aeolian transport serves as evidence of increased storminess dated between CE 0 and 650 (2.01 and 1.36 ka) which is coincident with the Dark Ages Cold Period (Jackson et al., 2005; Van Hengstum et al., 2015). In Puerto Rico and the Bahamas, coarse grain event deposits are dated between BCE 700 and CE 950 (2.71 and 1.06 ka) (Donnelly and Woodruff, 2007; Van Hengstum et al., 2014; Toomey et al., 2012; Van Hengstum et al., 2015).

The previously discussed studies also provide evidential data for a younger interval of increased storm activity in the North Atlantic. As part of the Nikitina et al. (2014) study, two erosional surfaces were dated at CE 1310 to 1480 (0.70-0.53 ka) and CE 1510 to 1630 (0.50-0.38 ka). The ages of these erosional surfaces coincide with the ages of overwash fans deposited in Brigantine, New Jersey and Whale Beach, New Jersey (Nikitina et al., 2014). At Whale Beach, Donnelly et al. (2001) used isotopic dating techniques to reconstruct the history of three storm-induced overwash deposits. The oldest was deposited between CE 1280 and 1440 (0.74-0.58 ka), another was deposited between CE 1700 and 1920 (0.31-0.09 ka), and the youngest was deposited in CE 1962 (0.05 ka) and was thought to be associated with the Ash Wednesday Nor'easter

34

of 1962. Donnelly et al. (2015) dated heightened frequency event bed deposits at CE 1390 to 1660 (0.62-0.35 ka). There is evidence of increased frequency of barrier island breaching in the Outer Banks of North Carolina during the same time period, from CE 1310 to 1710 (0.71-0.31 ka) (Mallinson et al., 2011). There are also similar event bed deposits found in the Bahamas and Mattapoisett Marsh, MA as well as extensive erosion events in Connecticut salt marshes between CE 1390 and 1660 (0.62 and 0.35 ka) (Donnelly et al., 2015). In the Buynevich et al. (2007) study, two relict scarps were dated were dated within this younger interval of increased storm activity in the North Atlantic. One relict scarp is dated at CE 1540 (0.47±0.03 ka). The event associated with this scarp may be related to an overwash deposit in Cape Cod, Massachusetts and is consistent with large flood events in Europe during the increased storminess of the Little Ice Age (Buynevich et al., 2007). Another relict scarp is dated at CE 1780 (0.23±0.03 ka). The age of this scarp is consistent with the Great Colonial Hurricane of 1635 (0.38 ka) or storms of 1638 (0.37 ka) (Buynevich et al., 2007). European sediment and stratigraphic data, as part of the Sorrell et al. (2012) study, reveals a Holocene storm period from CE 1340 to 1690 (0.6-0.32 ka). All late Holocene storm periods occur during spans of global rapid climate change with associated ocean and atmospheric reorganizations (Sorrell et al., 2012). Grain size data indicates increased storm activity in Bermuda from CE 1240 to 1840 (0.77-0.17 ka), Puerto Rico and the Bahamas from CE 1340 to 1590 (0.67-0.42 ka), NW France from CE 1340 to 1640 (0.67-0.37 ka), Iceland from CE 1440 to 1890 (0.57-0.12 ka), and the NW Mediterranean from CE 1540 to 1890 (0.47-0.12 ka) (Jackson et al., 2005; Donnelly and Woodruff, 2007; Sorrel et al., 2009, 2012; Toomey et al., 2012; Sabatier et al., 2012; Van Hengstum et al., 2015, 2014).

Some data along the southeastern coast of the United States do not quite align with the previously described periods of increased storminess. Culver et al. (2007) examined foraminiferal assemblages in the Outer Banks, North Carolina to discover that the Outer Banks experienced a collapse around CE 850 (1.16 ka) as a result of a major hurricane or a closely spaced series of major hurricanes. This study was supported by Mallinson et al. (2011) in which OSL dating of inlet-fill and flood tide delta deposits in the Outer Banks revealed evidence of storm impact from CE 480 to 1410 (0.61-1.54 ka). Furthermore, Timmons et al. (2010) age dated a bay ravinement surface in the Bogue Banks of North Carolina at around CE 850 (1.16 ka), which aligns directly with the findings of Culver et al. (2007). These data seem to be associated with the Medieval Warm Period, a time from CE 900 to 1100 (1.11-0.91 ka) characterized by relatively warm SSTs in the tropical North Atlantic and extended La Niña conditions (Mann et al., 2009).

# 4    Methods

## 4.1    Field Methods

The study site is located within Cape Henlopen State Park in Cape Henlopen, Delaware, USA. Cape Henlopen State Park provides excellent access to much of the modern and relict spit complex. During a one-week excursion to the study site, samples and data were collected using sediment cores and GPR.

### 4.1.1    Sediment Coring

Sediment coring sites were strategically chosen in an effort to sample the chronological advance of the spit complex from the oldest of the recurved spits to the youngest features of the beach accretion plain. Both a hand auger and a vibracoring system were used. Boreholes were initially hand augered down to the water table while logging sediment characteristics every 10 cm. The reason for this was to increase core penetration by beginning the vibracores at the water table instead of the ground surface. No sediments were collected from the hand auger. A total of 7 cores (Figure 20) were obtained throughout Cape Henlopen State Park. Rodding and bottom loss were common problems while vibracoring due to the nature of the sand size sediments. Handmade core catchers, constructed from sheet metal and rivets, were attached to the bottom of each vibracore pipe to prevent sediment loss upon retrieval. The final length of each sediment core after retrieval averages around 1-2 meters.

Each core was eventually split and photographed. The texture, organic content, color, and sorting was visually described every 10 cm. Samples for grain size analysis were taken every 10 cm. Samples for OSL dating were taken at depths within the cores that indicated spit beach sediments.

37

### 4.1.2   Ground Penetrating Radar (GPR)

GPR data was collected throughout Cape Henlopen State Park using a GSSI SIR-20 system with a 200-MHz antenna. Eighteen profiles (Figure 13) were collected for a total of approximately 10 km of trackline: (1) lines 1, 2, and 3 were test lines; (2) lines 4, 12, and 13 were collected perpendicular to the axes of relict recurved spits; (3) line 5 was collected perpendicular to the Great Dune and beach accretion plain; (4) line 6 was collected parallel to the beach accretion plain; (5) line 7 was collected south-north from the beach accretion plain to the modern simple spit; (6) lines 8-11 and 14-18 were collected parallel to the axes of relict recurved spits. GPS data was used to determine location along tracklines. Lines 4-7 were collected at 20 scans/m and lines 8-18 were collected at 40 scans/m.

ArcGIS and GSSI's Radan software were used to process the GPR data. In ArcGIS, USGS NED one-meter light detection and ranging (LiDAR) and GPS data were used to assign elevations to the GPR data. All elevation measurements refer to the North American Vertical Datum of 1988 (NAVD88). GSSI's Radan was used to process the GPR data with a (1) FIR filter; (2) gain; (3) surface normalization; (4) stack 2 or stack 4; (5) second FIR filter; and (6) second gain. Radar velocities measured using hyperbolic reflection patterns in the GPR data profiles yield around 0.2 m/ns in the upper portions of the profiles and around 0.09 m/ns in the lower portions of the profiles. A velocity of 0.15 m/ns, determined by evaluating hyperbolic reflections using Radan software, was used in time-to-depth conversions for more accurate values at the depths significant to this study. Due to software limitations, only one radar velocity was able to be applied to the time-to-depth conversions.

## 4.2    Laboratory Methods

### 4.2.1    Grain-Size Analysis

Samples for grain-size analysis were collected every 10 cm from each vibracore tube. The samples were dry sieved down to 2 mm. Grains exceeding 2 mm in diameter were documented and removed in order to run the samples through a CILAS 1190 Laser Particle Size Analyzer. Before use, the CILAS 1190 was calibrated using manufacturer-provided sand-sized glass calibration beads. GRADISTAT v8 was used to calculate sample statistics such as mean grain size, sorting, skewness, and kurtosis from the data obtained from the CILAS 1190.

### 4.2.2    Optically Stimulated Luminescence (OSL)

At least one sample was taken from each sediment core for OSL dating. Each sample consisted of a 15 cm section of sediment removed from a vibracore tube. Sample preparation was performed in a dark room laboratory fitted with amber and red lighting at Coastal Carolina University. The outer 2 cm of sediment in each sample was removed and used for dose rate calculations. The remaining sediment was wet-sieved using 125μm, 180μm, 250μm, and 355μm mesh sizes. The 125-180 μm-sized sediments were preserved as auxiliary material. The 250 μm-sized sediment was further processed for OSL measurements. Sodium polytungstate was used to remove heavy minerals and to separate quartz from feldspar.

SAR protocol was followed for OSL measurement (see Section 3.3) (Murray and Wintle, 2000; Murray and Wintle, 2003). Aliquots with the central ~1 mm diameter area masked by purified 180-250 μm quartz, approximately 17 quartz grains per disk, were

preheated at 160°C with a heating rate of 5°C/sec and stimulated with Blue LEDs for 40.0 s to produce OSL decay curves. When accepting aliquots, the background signal was estimated immediately following the initial signal. If insufficient bleaching was suspected, the minimum age model (MAM) was applied. The central age model (CAM) was applied if $D_e$ distribution and overdispersion suggested sufficient bleaching. All OSL measurement was performed in the luminescence dating laboratory at the University of Liverpool using a Risø DA-15 B/C reader equipped with 27 blue LEDs (470±30 nm) providing ~30mWcm$^{-2}$ at 90% power and 21 infrared LEDs (830±10 nm) providing ~110 mWcm$^{-2}$ at 90% power for optical stimulation. OSL and IRSL were detected through a 7.5 mm Hoya U340 filter (transmitting 320-390 nm).

The Risø Analyst program was used to analyze each aliquot. The signal integral was chosen to be from 1-3 seconds while the background integral was chosen to be from 4-11 seconds. This early background approach is to eliminate the contribution of slow components and results in less thermal transfer, less recuperation, and greater accuracy (Cunningham and Wallinga, 2010). The general criteria for accepting an aliquot included a recycling ratio value between 0.9 and 1.1 (Murray and Wintle, 2003), a recuperation value of 5% or less (Murray and Wintle, 2003; Preusser et al., 2008), and if the first test signal is less than 100 OSL counts per 0.16 seconds. An average of 29 aliquots were accepted per sample. Internal consistency was tested by OSL age dating two samples from the same sediment core (COSL45 and COSL46).

The natural radioactivity of the samples was measured with a high resolution and low background gamma spectrometer and converted to natural dose rate following Guérin et al. (2012) with the attenuation effect of water corrected following Aitken

(1985). An internal dose rate of 0.03±0.02 Gy/kyr was assumed. The attenuation of beta

irradiation was considered following Mejdahl (1979). The contribution of cosmic

radiation was calculated following Prescott and Hutton (1994). When calculating cosmic

radiation contribution, the depth of the sample must be considered. Sample depth

uncertainty was determined by calculating the shallowest and deepest possible depth for

each sample, taking the augering depth, rodding, and compaction of sediment inside the

vibracore pipe into consideration. All OSL ages are reported as before 2017 C.E.

(common era).

## 5    Results

### 5.1    Grain Size Analysis

Overall, the grain size samples analyzed (Figure 12) for this study align relatively

well with the grain size analyses of Kraft et al. (1978) and Maurmeyer (1974). All

samples are composed of sand-sized particles, each with a mean sediment size of coarse

sand (1.0-0.5 $\phi$). While samples are moderately to well sorted (0.8-0.4 $\phi$), numerous

samples are finely skewed. Organic matter is sparse and usually composed of woody and

root material. Gravels are also found in various samples, but they are seemingly more

common in samples of deeper depths. Grain size analysis was utilized for choosing the

depth of OSL samples in each core. Since the objective of this study is centered around

the ages of the spit beach sands, the OSL samples needed to be of beach quartz sand.

Ramsey (1999b) published a report on beach sand textures from the Atlantic coast of

Delaware which aided in sampling. The data of the Ramsey (1999b) report suggests that

the mean grain size of Delaware beach sand is 1.5-0.5 $\phi$, which is coarse to medium sand,

and the sorting is 0.5 or less $\phi$, which is well to very well sorted. The Cape Henlopen

OSL samples are congruent with the Delaware beach sand parameters.
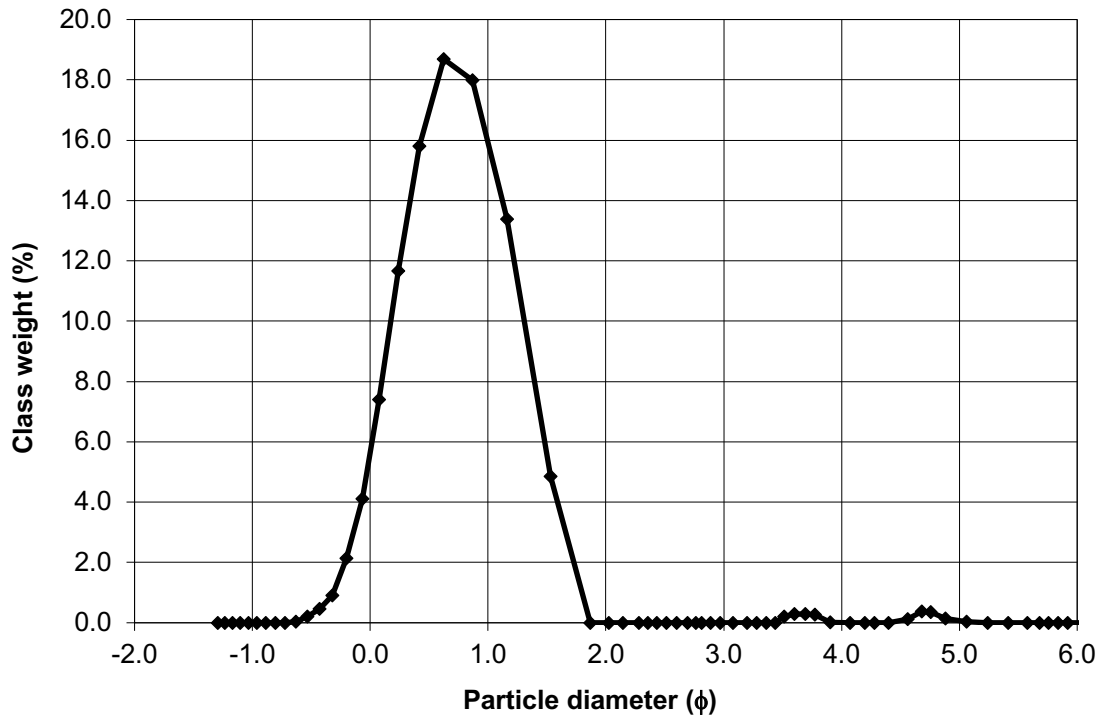


*Figure 12. Overall grain size distribution in phi ($\phi$). Grain sizes between 1.0 and 0.5 $\phi$ are dominant with evidence of fine skew.*

## 5.2 Ground Penetrating Radar (GPR)

The 15 GPR profiles run both parallel and perpendicular to recurved spit axes

(Figure 13). The 200 MHz antenna provided a penetration depth of around 12-15 m in

most areas; however, signal attenuation was an issue on the western ends of the relict

recurved spits due to saltwater intrusion or brackish porewaters. Throughout the relict

recurved spits and beach accretion plain are consistent boundary surfaces and facies

patterns. The boundaries present themselves as high amplitude, continuous, subhorizontal

reflections separating sedimentary facies in the GPR profiles. The sedimentary facies are

42

indicated by the radar facies patterns observed in the GPR data. The following radar facies are consistent throughout the study area: parallel facies, hummocky facies, oblique facies, and reflection-free facies. These facies are similar to those observed by Daly et al. (2002).

Transects that run parallel to spit axes typically display parallel and hummocky facies. In this instance the parallel facies can be either spit platform or spit beach deposits, depending on depth and orientation in relation to the boundary reflections. These parallel reflections are high amplitude, continuous, and nearly horizontal. Hummocky facies are interpreted as spit beach and dune deposits and are often discontinuous and low to medium amplitude. It is also common to see mounding and cross bedding in the hummocky facies. Transects that run perpendicular to spit axes typically display oblique and hummocky facies. The deepest set of oblique reflections, bounded on top and bottom by the continuous high-amplitude reflections, are interpreted as spit platform deposits. These reflections are often low to medium amplitude, moderately dipping, and continuous. The section of GPR profile beneath the lowermost bounding surface is reflection-free, which is assumed to be estuarine and lagoonal muds according to cross-sections created by Kraft et al. (1978). Overlying the upper bounding surface of the spit platform are more oblique facies reflections interpreted as spit beach deposits. These reflections are often medium to high amplitude, moderately dipping, and continuous. The spit beach facies, in some areas, may be bounded on top by a high amplitude subhorizontal reflection surface overlain by dune deposits (Figures 16 and 18). In other areas there is no top boundary and the dune deposits are directly adjacent to the spit beach deposits (Figures 14, 17, and 19). Depths associated with spit platform and spit beach sands contain instances of channels and channel fill

43

presented as v-shaped reflections in profiles. Channel and channel fill features are most prominent on the neck of the spit. There was little visible evidence of swash bar welding throughout the GPR profiles.

Roughly 1.2 km of GPR data was collected in the beach accretion plain. A majority of the transect was run parallel to the ridge axes. A continuous, high amplitude subhorizontal boundary surface is visible at -4 m (Figure 15). Below this boundary surface are low amplitude, continuous reflections that are parallel to gently dipping eastward toward the Atlantic. Hyperbolic reflections are common within this facies. These reflections are visible from -4 to -12 m and are interpreted as spit platform sands and gravels. Above the -4 m boundary surface are parallel and gently dipping reflections. The parallel facies are presented as medium to high amplitude, continuous, nearly horizontal reflections that extend from just beneath the ground surface to the -4 m boundary and are interpreted as spit beach sands. The parallel reflections begin gently dipping seaward in the eastern parts of the GPR profiles in the beach accretion plain. This is likely associated with the development of the cuspate spit after the recurved spit attached to the mainland. In some instances, the reflections dip gently landward and downlap onto the spit platform (e.g. the westward dipping reflection package seen in (Figure 15). These reflections are interpreted as overwash fan foresets associated with storm activity.

Twelve transects of GPR data were collected in the area of relict recurved spits. The four transects closest to the ends of the recurved spit tips were highly affected by rapid signal attenuation due to brackish porewaters or saltwater intrusion from Lewes Creek Marsh. However, transects to the east display signal penetration depths of up to 12 m beneath the ground surface. The same boundary reflection found in the beach accretion

plain, which separates the spit platform and the overlying spit beach sediments, is seen in the relict recurved spit tips at depths between -4 and -5 m (Figures 14, 16, 17, 18, and 19). The boundary is characterized as a continuous, high amplitude subhorizontal reflection.

Unlike the beach accretion plain, there is another, deeper boundary reflection at around -8.5 m. This boundary surface appears as a continuous, medium amplitude subhorizontal reflection and is interpreted as the division between underlying estuarine and lagoonal muds and overlying spit platform sands and gravels. The estuarine and lagoonal muds are reflection-free. The spit platform sands and gravels are characterized by low to medium amplitude, continuous, parallel reflections in transects parallel to spit axes. In transects perpendicular to spit axes (Figure 18) the spit platform deposits are characterized by low to medium amplitude, continuous, oblique, gently dipping reflections with sporadic higher amplitude hyperbolic reflections. The spit platform facies occurs between approximately -4 to -8.5 m and is bounded on top and bottom. Above the spit platform's upper boundary are continuous, high amplitude parallel and oblique reflections interpreted as spit beach and dune sands, similar to those found in the beach accretion plain. This facies occurs between the ground surface and -4 m. In some of the profiles (e.g. Figures 16 and 18) there are high angle reflections downlapping directly onto the spit platform boundary, which are similar to the landward dipping reflections found in the beach accretion plain (Figure 15). These reflections are interpreted as overwash fan foreset deposits, most likely associated with overwash fan migration and storm activity. Their steep reflection angles indicate these sediments may have been deposited into a body of water on the landward side of the recurved spit (Schwartz 1982).
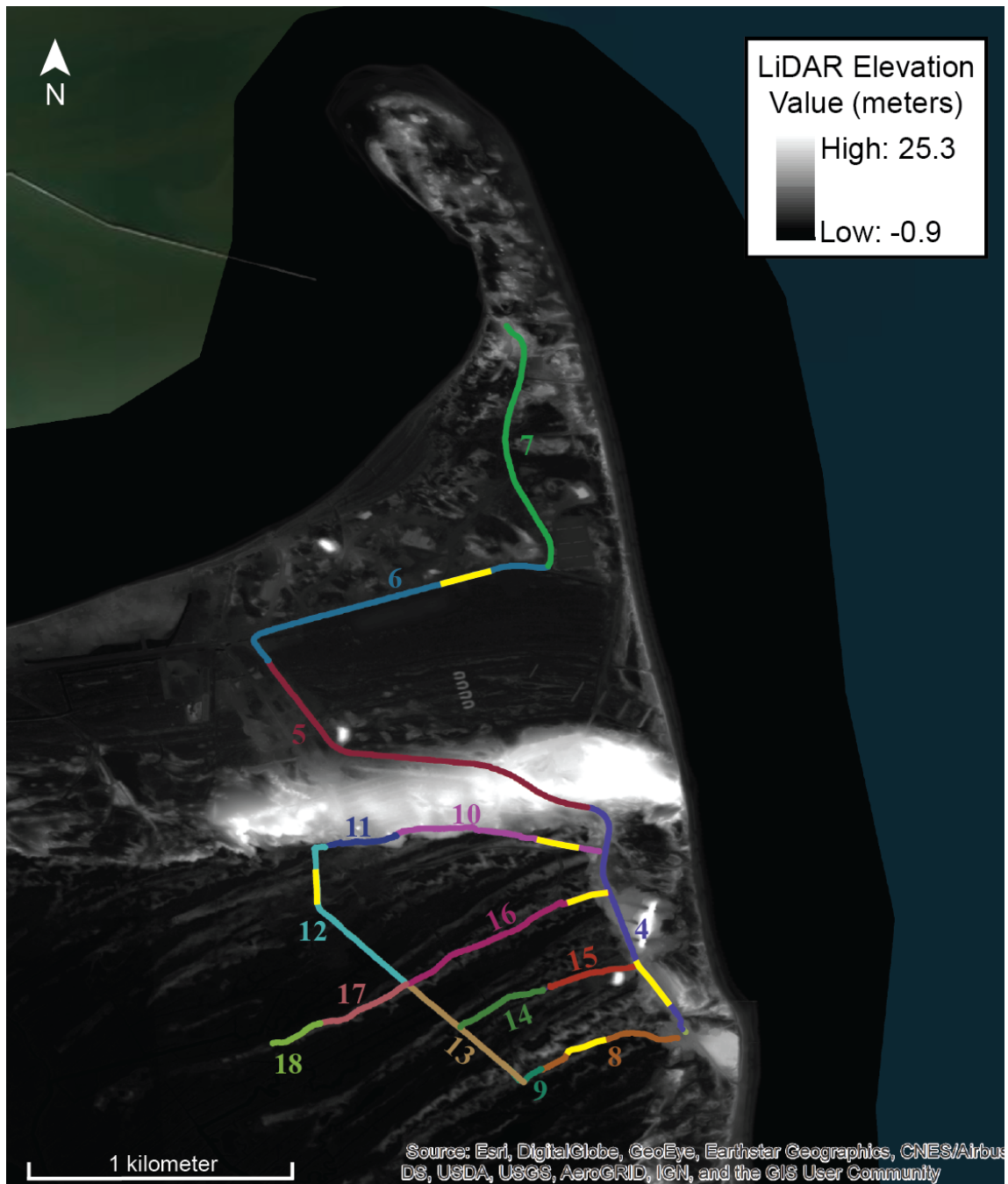
*Figure 13. LiDAR map of Cape Henlopen with GPR transect locations. The locations of the following GPR profile figures are highlighted in yellow on their respected GPR transect.*
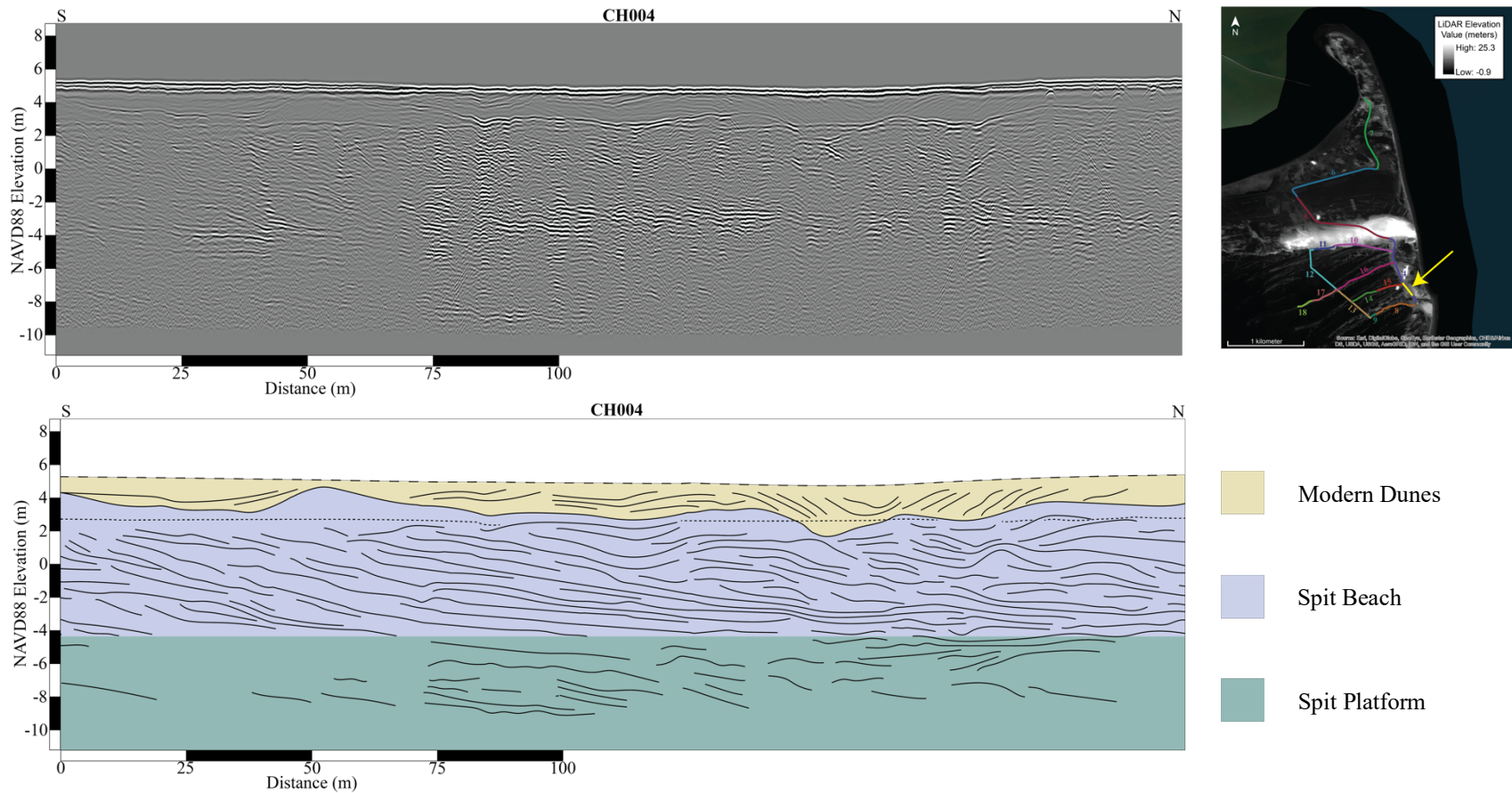
*Figure 14. GPR profile and interpretation for the CH004 transect running south to north parallel to the axis of the neck of the relict recurved spit and perpendicular to the recurved spit tips. The dashed line indicates the ground surface and the dotted line indicates what is interpreted as the water table. Channeling and overwash scours are common at the base of the aeolian sediments between 1 and 4 m throughout the transect. There is a boundary at -4 m that separates the spit beach sands and the spit platform sands and gravels. The oblique reflections in A and B gently dip northward, the direction of spit growth. Modern sand dunes comprise the uppermost 2 m of this profile.*
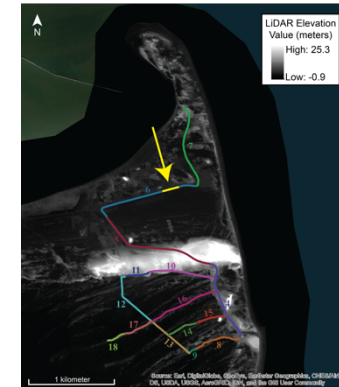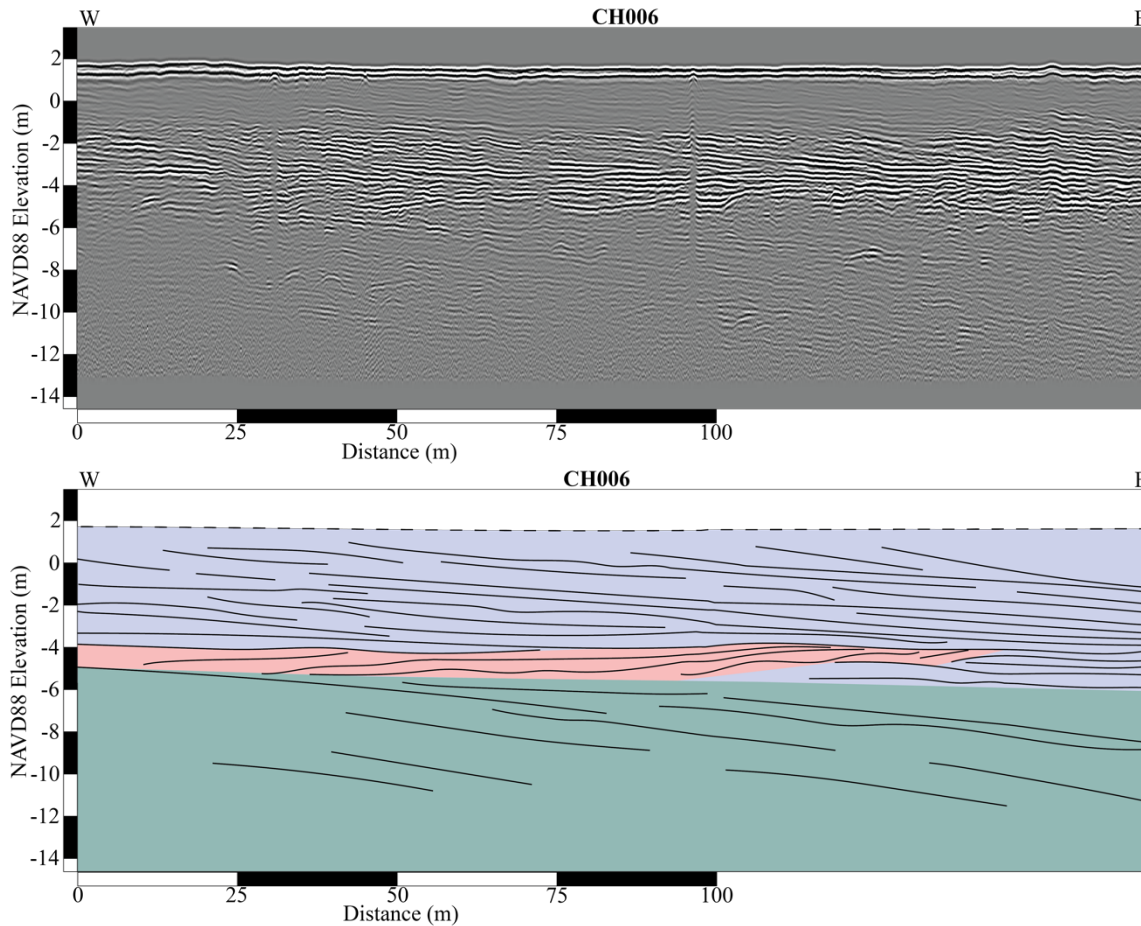
*Figure 15. GPR profile and interpretation for the CH006 transect running west to east parallel to the axis of the beach accretion plain. The dashed line indicates the ground surface. There is a boundary at -5 m separating the spit beach sands and the spit platform sands and gravels. Most reflectors dip slightly east toward the Atlantic Ocean which may be associated with the growth of the cuspate spit after the recurved spit joined with the mainland. A wedge of gently dipping, westward reflections is present between -4 and -5 m. These reflections downlap onto the spit platform and are interpreted as overwash fan foresets.*
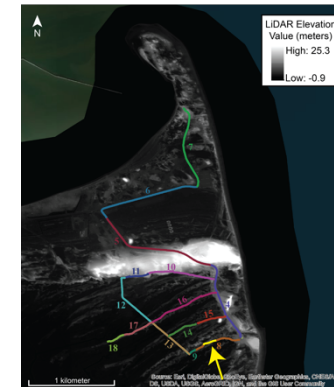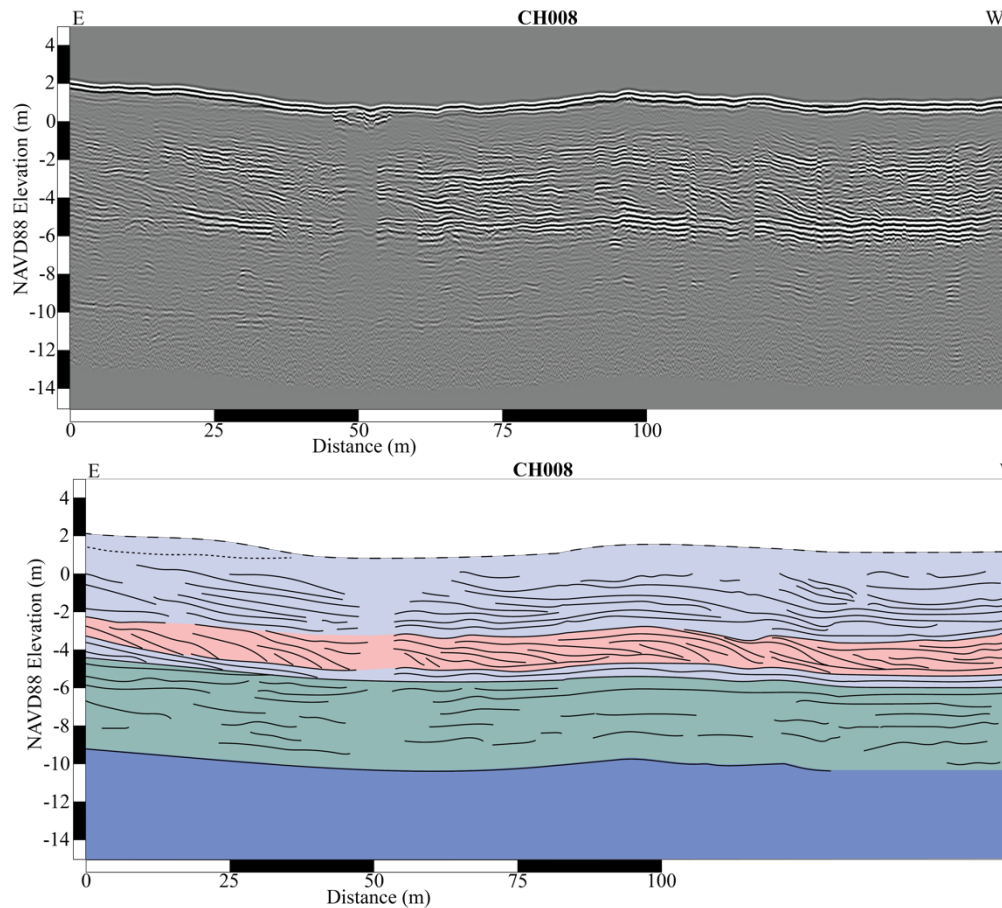
*Figure 16. GPR profile and interpretation for the CH008 transect running east to west parallel to the axis of the relict recurved spit. The dashed line indicates the ground surface and the dotted line indicates what is interpreted to be the water table. There is a boundary at -5 m separating the spit beach sands and the spit platform sands and gravels. There is also a boundary at -10 m separating the spit platform sediments and the shallow marine sediments. Most reflections are parallel, except for a package of reflections of various dipping angles that downlap onto the boundary at -5 m. These are interpreted as overwash fan foresets associated with the progradation of the recurved spits.*
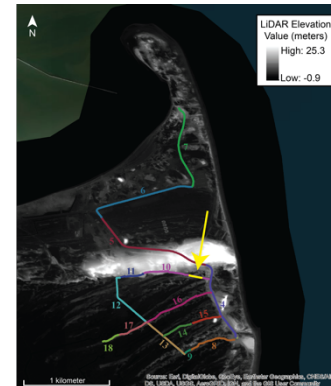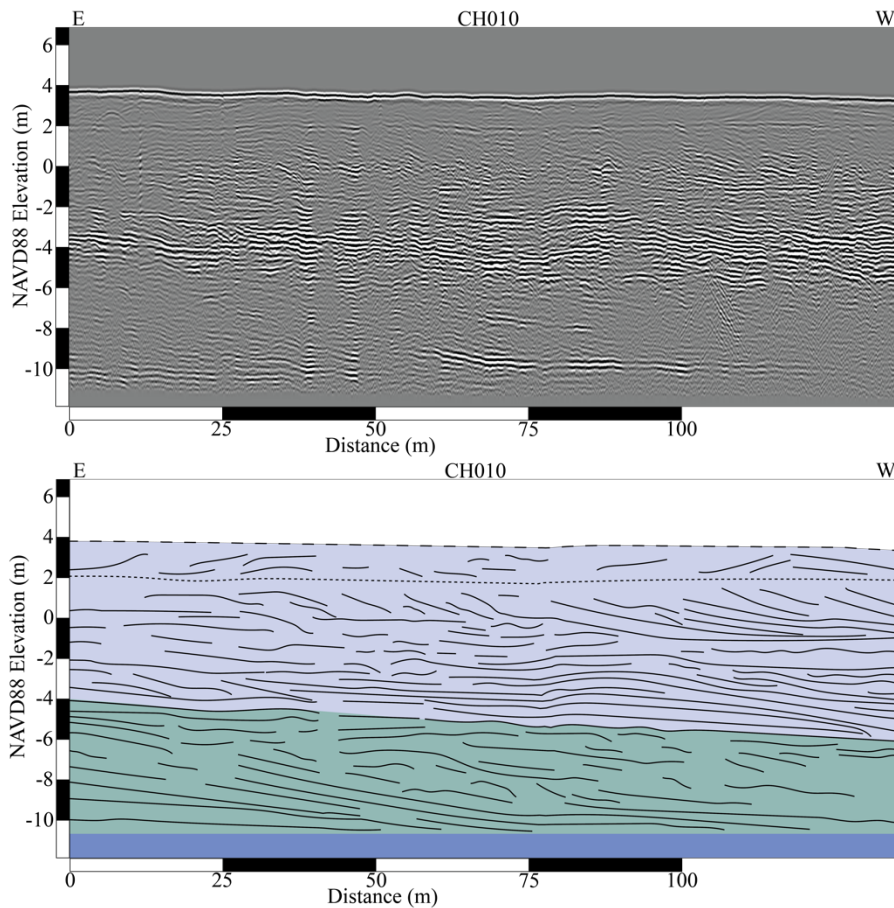
*Figure 17. GPR profile and interpretation for the CH010 transect running east to west parallel to the axis of the relict recurved spit. The dashed line indicates the ground surface and the dotted line indicates what is interpreted to be the water table. There is a boundary at -5 m separating the spit beach sands and the spit platform sands and gravels. There is also a boundary at -10 m separating the spit platform sediments and shallow marine sediments. CH010 displays very similar features to CH008 and is evidence for the consistency of boundary and facies depths throughout the recurved spits.*
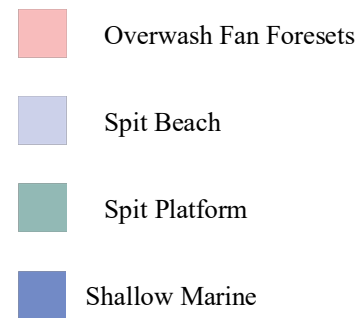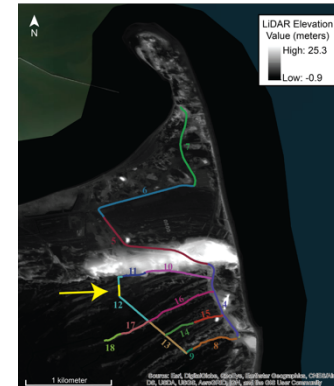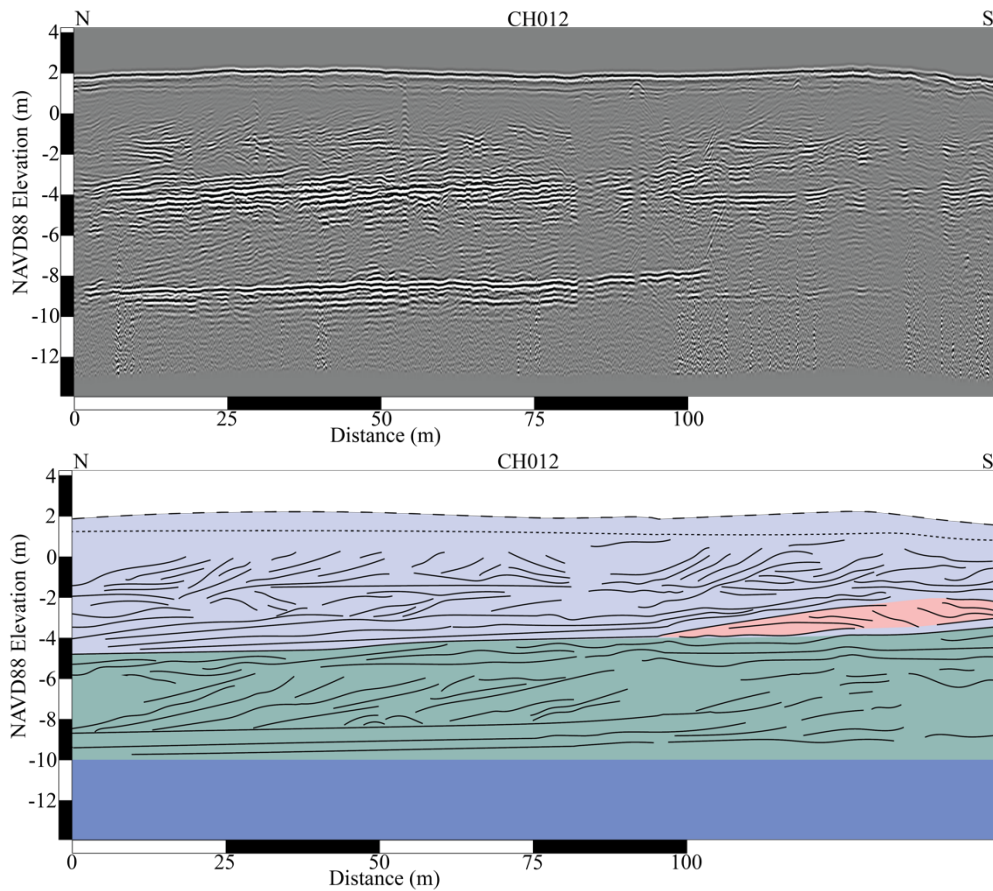
*Figure 18. GPR profile and interpretation for the CH012 transect running north to south perpendicular to the axis of the relict recurved spit. The dashed line indicates the ground surface and the dotted line indicates what is interpreted to be the water table. There is a boundary at -4 m separating the spit beach sands and the spit platform sands and gravels. There is also a boundary at -9 m separating the spit platform sediments and shallow marine sediments. Channeling is present between recurved spit tips. The reflections composing the spit beach and platform facies are gently to moderately dipping northward except for a package of south-dipping reflectors between -3 and -4 m. This package is interpreted to be overwash fan foresets.*
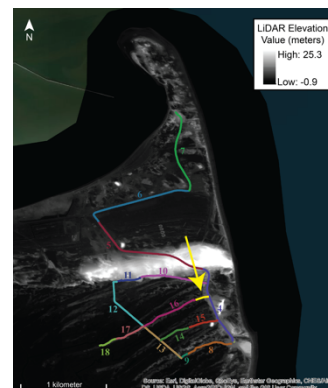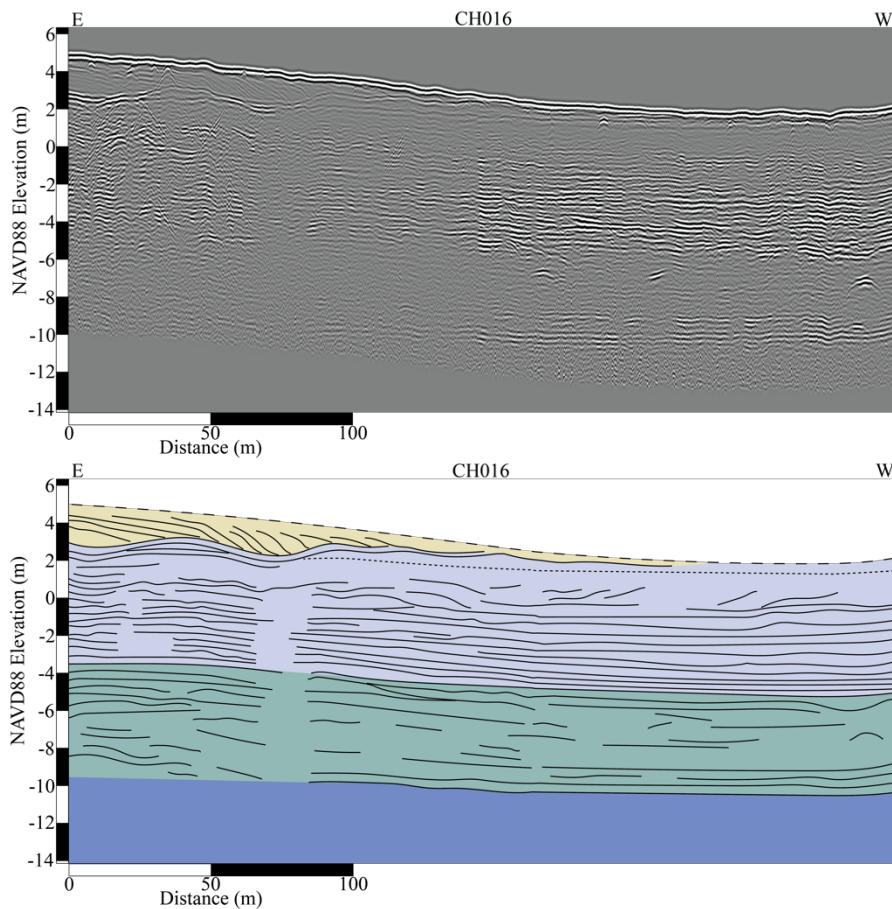
*Figure 19. GPR profile and interpretation for the CH016 transect running east to west parallel to the axis of the relict recurved spit. The dashed line indicates the ground surface and the dotted line indicates what is interpreted to be the water table. There is a boundary at -4 m separating the spit beach sands and the spit platform sands and gravels. There is also a boundary at -10 m separating the spit platform sediments and shallow marine sediments. Channeling is present in the eastern portion of the profile where the transect intersects part of the neck of the recurved spit.*

## 5.3    Optically Stimulated Luminescence (OSL)

A total of 8 OSL ages were acquired from the relict recurved spits and beach accretion plain of Cape Henlopen (Figure 20 and Table 1).
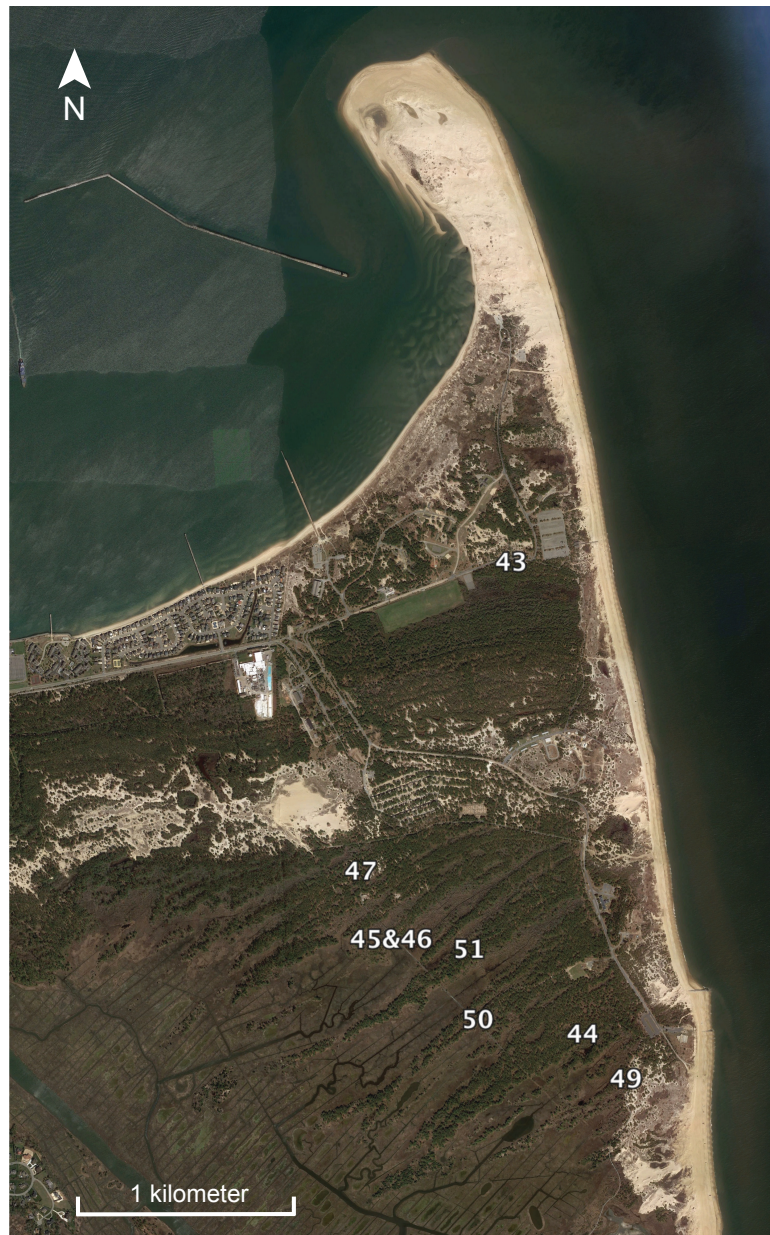


*Figure 20. Satellite image of Cape Henlopen with the locations of each OSL sample. See Table 1 for sample ages.*

| Sample | Min. Grain Size | Max. Grain Size | $D_e$ | $\delta D_e$ | Dose | $\delta$ Dose | Age | $\delta$ Age | Error |
|--------|------------------|------------------|-------|---------------|------|----------------|-----|---------------|-------|
| | μm | μm | Gy | Gy | Gy/ka | Gy/ka | ka | ka | % |
| COSL43 | 180.00 | 250.00 | 0.270 | 0.030 | 0.498 | 0.047 | 0.54 | 0.08 | 14.62 |
| COSL47 | 180.00 | 250.00 | 0.710 | 0.030 | 0.469 | 0.041 | 1.52 | 0.15 | 9.68 |
| COSL46 | 180.00 | 250.00 | 0.800 | 0.040 | 0.500 | 0.047 | 1.60 | 0.17 | 10.72 |
| COSL45 | 180.00 | 250.00 | 0.930 | 0.080 | 0.575 | 0.053 | 1.62 | 0.20 | 12.56 |
| COSL51 | 180.00 | 250.00 | 0.830 | 0.060 | 0.492 | 0.047 | 1.69 | 0.20 | 12.02 |
| COSL50 | 180.00 | 250.00 | 0.940 | 0.040 | 0.505 | 0.047 | 1.86 | 0.19 | 10.18 |
| COSL44 | 180.00 | 250.00 | 0.960 | 0.050 | 0.515 | 0.042 | 1.86 | 0.18 | 9.64 |
| COSL49 | 180.00 | 250.00 | 1.040 | 0.040 | 0.436 | 0.040 | 2.39 | 0.24 | 10.00 |

*Table 1. Calculated ages and errors of each OSL sample collected in Cape Henlopen. The youngest sample, COSL43, was collected in the beach accretion plain. The oldest sample, COSL49, was collected in the oldest section of relict recurved spits. COSL45 and COSL46 were sampled from the same core. Equivalent dose ($D_e$) values and dose rate values are also displayed.*

The OSL sensitivity was calculated for each sample (Figure 21) using the test dose signal value of each aliquot, modelled after a similar figure in McKeever (2001). This figure provides a visual of how homogeneous each sample is in terms of how many aliquots produce a measurable amount of OSL signal. As explained in Duller (2008), not all grains luminesce; in fact, only 1-20% of the grains in each aliquot actually produce a measurable signal. This variation in sensitivity can be seen in Figure 21 between, for example, COSL43 and COSL49. A steeper curve, such as the curve for COSL43, is indicative of a less homogeneous sample. In other words, few aliquots produced a measurable OSL signal. In contrast, the less steep curve of COSL49 is indicative of a more homogeneous sample where a greater number of aliquots produced a measurable OSL signal. The samples with steeper curves may yield results more similar to single-grain OSL analyses, even though tens of grains composed each aliquot.
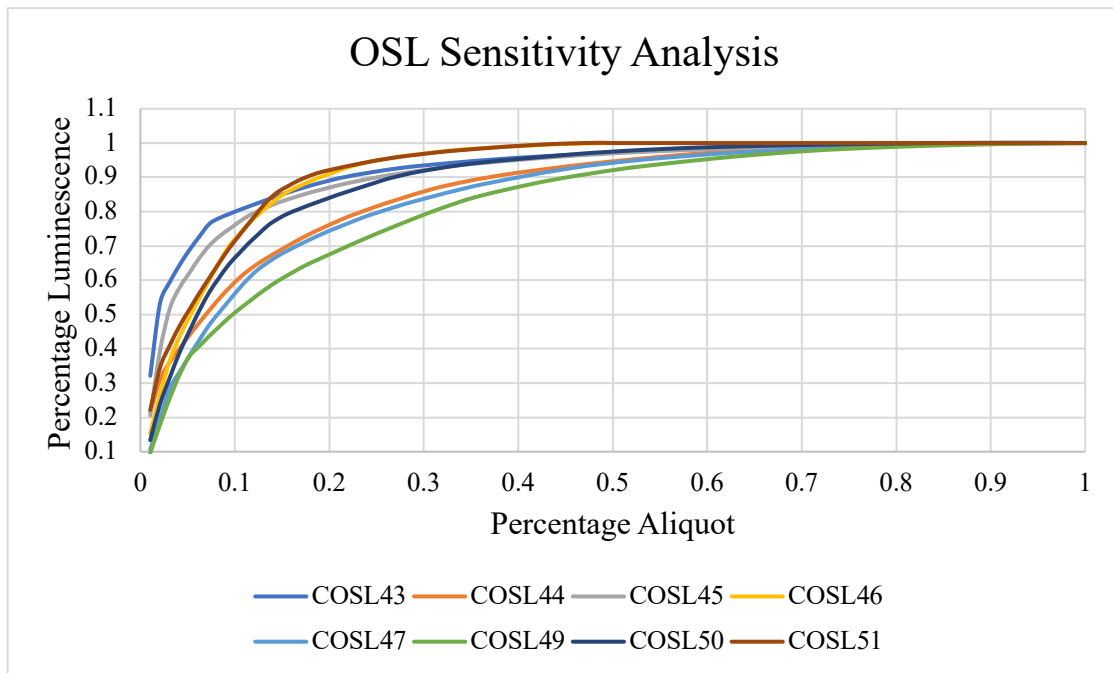
*Figure 21. Plot of OSL sensitivity for each OSL sample. Steeper curves indicate a less homogeneous sample; less aliquots produce a measurable OLS signal. Less steep curves indicate a more homogeneous sample; more aliquots produce a measurable OSL signal.*

One goal of this study was to age date the succession of relict spit features between the radiocarbon dates obtained by Kraft and Hiller (1987). Kraft and Hiller (1987) dated the oldest of the recurved spits as approximately BCE 500 (2.5 ka) and the youngest of the spit features in the beach accretion plain as approximately CE 1500 (0.5 ka). The oldest and youngest OSL ages align well with the ages calculated by Kraft and Hiller (1987). The oldest OSL age, COSL49, was calculated at BCE 370 (2.39±0.24 ka) and the youngest, COSL43, was calculated at CE 1480 (0.54±0.08 ka). It is important to note that OSL ages are not reported in years BP, they are reported in years before the measurement was taken. In the case of this study, OSL measurements were performed in CE 2017.

Around 0.3 km north-northwest of COSL49, COSL44 was dated at CE 160 (1.86±0.18 ka). Between COSL44 and COSL47/COSL48 the OSL ages are significantly close in age when compared to the age gaps between COSL49-COSL44 and between COSL47/COSL48-COSL43. In the span of approximately 1.25 km from COSL44 to COSL47/COSL48, the ages range from CE 160 (1.86±0.18 ka) to CE 500 (1.52±0.15 ka). Yet, in the span of approximately 0.3 km between COSL49 and COSL44 the ages lap from BCE 380 (2.39±0.24 ka) to CE 160 (1.86±0.18 ka). The clustering of relict spit ages suggest that the evolution of the spit complex is episodic.

## 6    Discussion

Storms have been proposed as a viable mechanism for spit growth in various studies. Scheffers et al. (2012) compiled evidence from numerous studies of storm influence on coastal barrier systems. Observations indicate that while high-category hurricanes are destructive, lower magnitude storms or distant high-magnitude storms can be very constructive. Perhaps storms provide increased sediment mobilization from eroding headlands or offshore sources, driving rapid, episodic spit extension (Ashton et al., 2016; Wright et al., 2018). For example, Long Bay, a coastal embayment between Cape Fear, North Carolina and Cape Romaine, South Carolina, experiences sediment mobilization induced by storm waves eroding shorelines and paleo-barrier systems (Wright et al., 2018).

Evidence of storm influence is found in the Cape Henlopen GPR data (Section 4.2). Channeling is found in sections parallel to the Atlantic coast, possibly due to overwash scouring from storm surges. It also appears that multiple relict recurved spits have packages of steeply dipping GPR reflections, resembling those described in Schwartz (1982), Fruergaard et al. (2015), and Montes et al. (2018), indicative of washover fan foresets associated with migrating washover fans. In each instance, these reflections downlap onto the boundary separating the spit platform and the overlying spit beach deposits. These reflections do not, however, continue throughout the entire profiles. They appear to "flatten out" and become nearly horizontal in some areas. This alternation between horizontal and steeply dipping reflections may indicate episodic storm events, or perhaps even storm periods. While there is no discernable evidence of swash bars or swash bar welding in the Cape Henlopen GPR profiles, it is still possible

that swash bar accretion played some role in the overall growth of Cape Henlopen, which is primarily driven by littoral transport (Maurmeyer, 1974; Kraft et al., 1978). Kraft (1971) supported the theory that a portion of the sediment deposited on the spit was/is derived from a storm-expanded offshore bar.

The extensional processes, being littoral transport and possible swash bar accretion, of the Cape Henlopen spit as imaged in GPR data share similarities with GPR-based models such as those suggested by Costas and FitzGerald (2011), Tillmann and Wunderlich (2013), and Wright et al. (2018). Costas and FitzGerald (2011) used GPR collected with a 200 MHz antenna along with drill cores to analyze the internal architecture and stratigraphy of the Merrimack River Inlet and Salisbury Spit along the northern coast of Massachusetts. The Costas and FitzGerald (2011) GPR revealed constructive phases marked by deposits of swash bars and foreshore cross-bedding deposits associated with the southerly longshore transport of sediment. While swash bar welding was considered a significant process of spit evolution, Costas and FitzGerald (2011) determined that linear downdrift sediment transport and deposition were the dominant processes of spit extension. Tillmann and Wunderlich (2013) reconstructed the geological development of the southern barrier spit located on the island of Sylt in the German North Sea using GPR collected with a 200 MHz antenna and shallow sediment cores. In this study, Tillmann and Wunderlich (2013) observed that progradation of the southern spit occurred episodically, when the sand supply was abundant. Tillmann and Wunderlich (2013) attribute this periodicity to severe storm surges that cause extensive erosion of updrift sediment sources (an unconsolidated moraine cliff in this particular study) which releases large amounts of sediment into the littoral system. Wright et al.

(2018) had similar observations while investigating the North Island sand spit located at the southern downdrift end of the Grand Strand coastline in NE South Carolina using GPR ground-truthed by vibracore and OSL age dating. Comparable to the Tillmann and Wunderlich (2013) and the Wright et al. (2018) studies, episodic advancement was recognized and may also be attributed to changes in updrift sediment supplied by longshore transport.

The Cape Henlopen spit has not always experienced a linear growth rate. Figure 22 displays the ages of the OSL samples plotted against distance to the southernmost and oldest sample, COSL49. Distance was calculated using satellite imagery to measure from one sampled recurved spit to the next starting with the southernmost, oldest sample and progressing northward to the youngest sampled ridge in the beach accretion plain. It is important to note that distance was not measured from one sample site to the next. Instead, since the sample sites vary in terms of how close they are to the ends of the recurved tips, the distances between the recurved spits themselves were used. This was done to avoid potential error; for example, if one recurved spit had a sample near the terminated end and an adjacent recurved spit had a sample far from the terminated end then the calculated distance between the samples would be much greater than the actual distance between the two recurved spits. It is assumed that individual points along each single recurved spit are fairly close in age. A steep slope between two sample data points indicates a slower spit growth rate while a shallow slope indicates a faster spit growth rate. The data in Figure 22 plots in a stairstep-like manner. COSL49 documents the recurved spit in its early stage after evolving from sandy barriers located against the Pleistocene headlands (Kraft et al., 1978). The steeper slope between COSL49 and

COSL44 as well as COSL47 and COSL43 suggests that the spit experienced a reduced

growth rate during those time periods. In contrast, the slopes between the sample data

points from COSL44 to COSL47 are quite shallow, suggesting the spit experienced an

increased growth rate within that time period. COSL44, 50, 51, 45, 46, and 47 are all

associated with prograding relict recurved spit ends. These samples are noticeably

clustered in age, ranging from only CE 160 to 500 (1.86-1.52 ka) over a distance of

about 1.3 km. It is important to note that COSL43, the youngest sample, was obtained in

the beach accretion plain and not the relict recurved spits like the other samples. Also, the

relict recurved spits between COSL47 and COSL43 are currently buried beneath the

Great Dune, preventing them from being sampled via vibracore for OSL age dating.

Nevertheless, there is an evident reduction in spit growth rate between COSL47 and
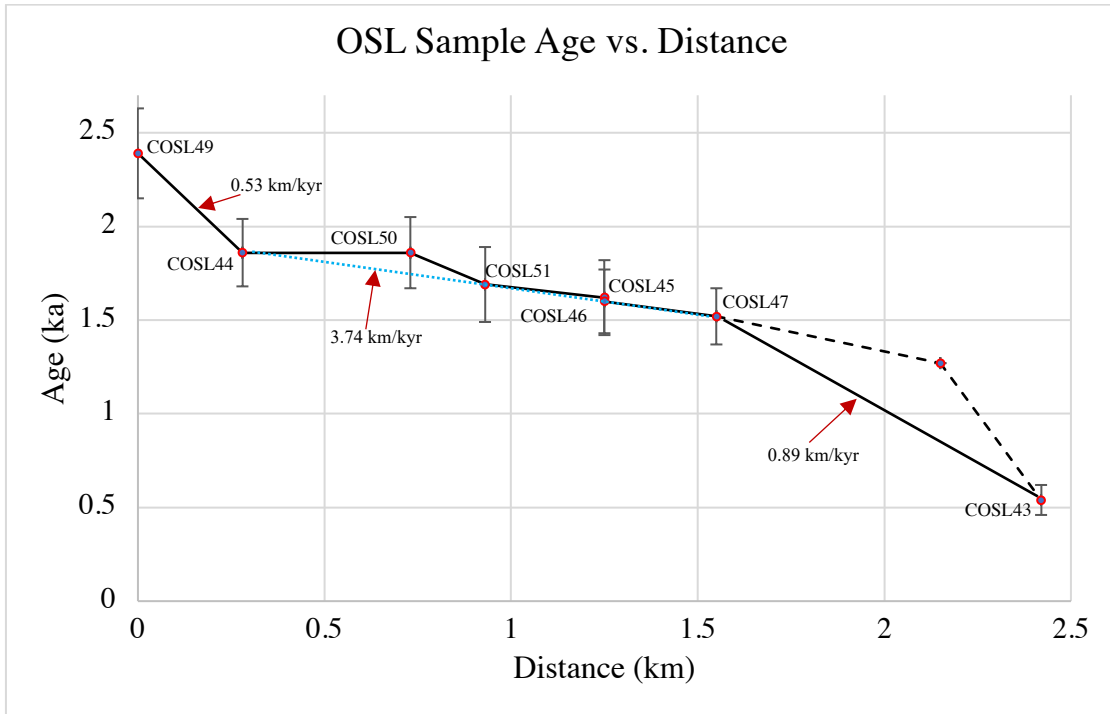


*Figure 22. OSL age dates for vibracore samples plotted against distance from the southernmost, oldest sample to the northernmost, youngest sample. The dashed line and unlabeled point represent the projected age and distance of the youngest of the relict recurved spits. The blue dotted line is a linear fit line between COSL44 and COSL47 (characterized by a clustering of OSL ages within the relict recurved spits). Progradation rates are included and are indicated by a red arrow.*

COSL43, which may be even more pronounced if OSL data beneath the Great Dune were available. An extra point was added to Figure 22 as an estimate age for the youngest of the recurved spits bordering the beach accretion plain. This was calculated by projecting the average growth rate of the other recurved spits beyond the Great Dune and to the youngest of the recurved spits. By doing so, the stairstep pattern becomes even more pronounced and the growth rate slope between the recurved spits and the beach accretion plain (COSL43) becomes steeper. The progradation rate for each apparent segment of growth was included in Figure 22 to further show the overall episodic, non-linear growth pattern of the spit complex. The progradation rate between COSL49 and COSL44 was 0.53 km/kyr, the slowest of the calculated progradation rates. A linear fit line between COSL44 and COSL47 was used to calculate the progradation rate between the samples with clustered ages, the result being 3.74 km/kyr, the most rapid of the calculated progradation rates. Finally, the progradation rate between COSL47 and COSL43 was calculated at 0.89 km/kyr. The differences in the progradation rates signifies episodic growth in the history of the Cape Henlopen spit complex.

When plotting the elevation of the spit platform surface against age (Figure 23), a somewhat linear trend becomes evident. The oldest sample located on a GPR transect, COSL44, is associated with a spit platform surface elevation of about -3.9 m whereas the youngest sample located on a GPR transect, COSL43, is associated with a spit platform surface elevation of about -5 m. The rest of the samples in the relict recurved spit area are associated with spit platform surface elevations around -4 to -4.1 m. This pattern may provide evidence against the theory proposed by Meistrell (1972), which proclaims that the spit platform always develops to a certain water depth and may be used to trace sea

61

level change. It would be expected that as sea level rises, the elevation of the spit platform surface would rise accordingly. However, the data in Figure 23 displays the opposite; the youngest sample is associated with a spit platform surface of lower elevation than the older samples which seems to imply an inverse relationship. Perhaps the spit platform surface elevation is not as dependent on sea level as previously thought, or perhaps other external factors have significant influence on the boundary elevation.
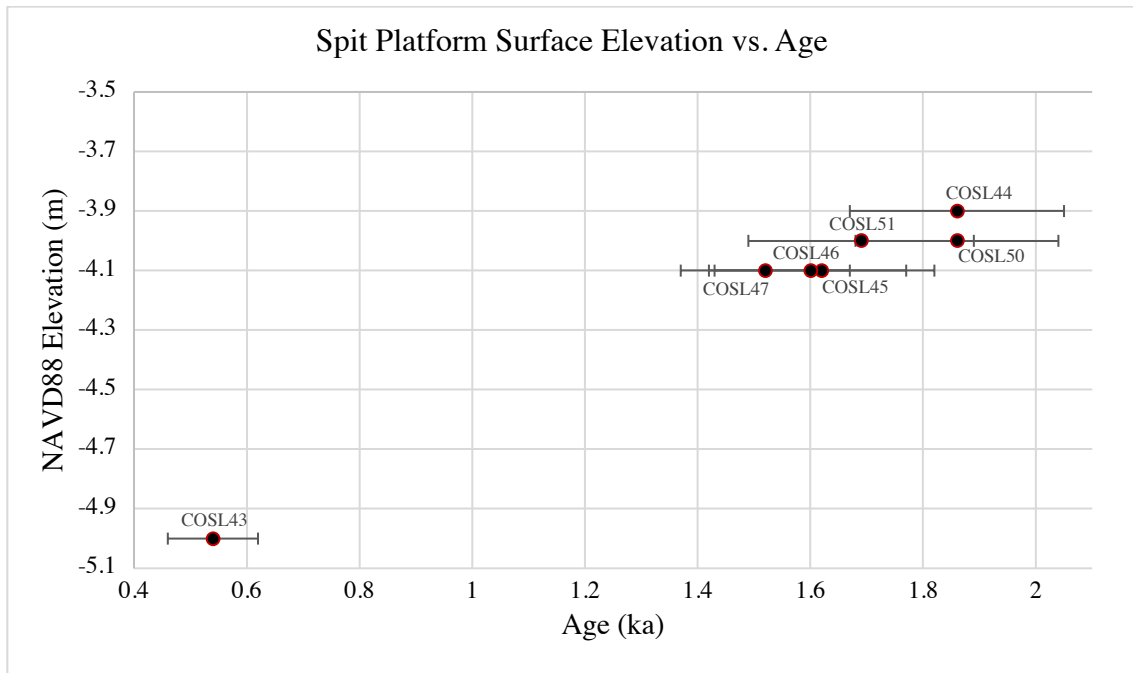


*Figure 23. Elevation of the spit platform surface boundary plotted against vibracore sample OSL age dates.*

The clustering of the ages of the relict Cape Henlopen spit features implies that spit evolution may be significantly influenced by intermittent events, such as storms. When comparing the Cape Henlopen OSL ages with an Atlantic storm record compilation (Section 2.4) a relationship between the ages of spit features and periods of increased northern Atlantic storm activity becomes evident (Figure 24). There is concurrent storm record data between Delaware (Nikitina et al., 2014), Maine (Buynevich et al., 2007), Massachusetts (Donnelly et al., 2015), Bermuda (Van

Hengstum et al., 2015), Puerto Rico (Donnelly and Woodruff, 2007), Bahamas (Van Hengstum et al., 2014; Toomey et al., 2012), Iceland (Jackson et al., 2005), NW Mediterranean (Sabatier et al., 2012), and NW France (Sorrel et al., 2009, 2012). All but one, the oldest (COSL49), of the Cape Henlopen OSL dates concurs with these two periods of increased northern Atlantic storm activity.

The two periods of increased late Holocene storm activity coincide with established climatic events. All late Holocene storm periods seem to occur during spans of rapid global climate change with associated ocean and atmospheric reorganizations (Sorrell et al., 2012). The span of CE 250 1150 (1.76-0.86 ka) is characterized with relatively warm sea surface temperatures in the main development region of the North Atlantic (Donnelly et al., 2015). This concurs with the Dark Ages Cold Period (DACP), affiliated with increased storm activity, from CE 50 to 750 (1.96-1.26 ka). The DACP is regarded as a period characterized by colder climate, hydroclimatic changes, and glacier advances around the Northern Hemisphere, including North America and Europe (Helama et al., 2017). The DACP is correlated with the 1500-year cycle of ice rafted debris deposition and cooling in the North Atlantic region from CE 50 to 550 (1.96-1.46 ka) (Bond et al., 1997, 2001; Sabatier et al., 2012) which is associated with reduced Atlantic Meridional Overturning Circulation (AMOC) (Van Hengstum et al., 2015). Reduced AMOC increases meridional temperature gradients and atmospheric baroclinicity which can increase extratropical cyclogenesis, according to models produced by Shaffrey and Sutton (2006). Unfortunately, regional paleoclimate studies are far less abundant for the DACP compared to the Little Ice Age (LIA) (Bradley and Jones, 1992, 1993; Matthews and Briffa, 2005; Helama et al., 2017).

The LIA was characterized by strong meridional atmospheric circulation and North Atlantic sea surface temperatures (SST) up to 1°C below modern SSTs (Keigwin, 1996). During the onset of the LIA from CE 1380 to 1650 (0.63-0.36 ka), a warm sea surface temperature anomaly in the western North Atlantic caused a southerly shift of the Intertropical Convergence Zone (ITCZ) which is thought to have increased hurricane genesis near the southeastern coast of the United States (Lund et al., 2006; Donnelly et al., 2015). Ice core data revealed evidence of increased meridional circulation, strengthened westerlies, and increased storminess throughout the North Atlantic (O'Brien et al., 1995; Mayewski et al., 2004) and lake records in Noren et al. (2002) provide additional evidence for increased storminess in the northeast U.S. during the LIA. While tropical storms and cyclones were likely contributors to the increase in storminess during the LIA (Van Hengstum et al., 2015), climatic and meteorological conditions likely favored extratropical storms (Davis and Dolan, 1992, 1993; Keim et al., 2004; Mallinson et al., 2011). Heightened production of powerful low-pressure systems on the U.S. east coast resulted from the increased meridional circulation and westerlies intensifying the jet stream and causing profound temperature gradients across weather fronts (Davis and Dolan, 1992, 1993; Keim et al., 2004). A product of such conditions is Nor'easters, which are storm systems characterized by sustained winds, initially east-northeast followed by west-southwest, that may exceed 74 km/hr and impact the entire U.S. east coast for up to several days (Mallinson et al., 2011). In addition, the LIA likely experienced AMOC conditions similar to the DACP (Van Hengstum et al., 2015).

In contrast, some studies (Culver et al., 2007; Timmons et al., 2010; Mallinson et al., 2011; Wright et al., 2018) found evidence of storms inbetween the interpreted periods

of increased storminess in Figure 24. The findings of the aforementioned studies align with the Medieval Warm Period (MWP). The MWP was characterized by relatively warm SSTs in the tropical North Atlantic and extended La Niña conditions from CE 900 to 1100 (1.11-0.91 ka) (Mann et al., 2009). It is possible that during this time tropical cyclones were more prevalent than extratropical cyclones and the tropical cyclones may have been directed more toward the southeast US and Gulf of Mexico. It is important to note that the author is not stating that there was no storm activity present in the North Atlantic inbetween the interpreted periods of increased storminess.

Additionally, the North Atlantic Oscillation (NAO), defined as the difference in atmospheric pressure at sea level between the Icelandic low and the Azores high, is a prominent topic when discussing storm activity since it dictates the strength and direction of storm tracks across the North Atlantic (Hurrell et al., 2003; Andrade et al., 2008; Hurrell and Deser, 2009; Olsen et al., 2012). However, several aspects make the NAO an unreliable factor to explain storm activity for this study. NAO reconstructions are limited to the past 900 years (Trouet, 2009) and exhibit decadal variability (Hurrell et al., 2003), where this study examines the past 2500 years on a centennial timescale. Also, NAO variability alone cannot explain the total history of North Atlantic cyclones (Mailier et al., 2006; van Hengstum et al., 2015).

While GPR and OSL were only collected in the relict recurved spits and beach accretion plain for this study, previous geological work by Kraft et al. (1978) can be used to briefly compare the modern simple spit with storm history to see if the positive relationship between storm activity and spit evolution applies. Kraft et al. (1978) states that the currently active simple spit at Cape Henlopen has advanced over 2 km since CE 1700

(0.31 ka). From about CE 1965 (0.05 ka) to the time of the Kraft et al. (1978) study (0.04 ka) the simple spit had accreted over 50 m of sediment per year to the north-northwest. Long-term Atlantic tropical cyclone activity trends produced by Mann et al. (2009) indicate a stark increase in cyclone frequency beginning around CE 1700 (0.31 ka) and another remarkable increase since CE 1900 (0.11 ka). These periods of increased tropical cyclone frequency align well with the advancement history of the Cape Henlopen simple spit determined by Kraft et al. (1978), thus providing even further evidence of a positive relationship between increased storminess and spit growth.

Age (ka)

| | 0-0.2 | 0.2-0.4 | 0.4-0.6 | 0.6-0.8 | 0.8-1.0 | 1.0-1.2 | 1.2-1.4 | 1.4-1.6 | 1.6-1.8 | 1.8-2.0 | 2.0-2.2 | 2.2-2.4 | 2.4-2.6 | 2.6-2.8 |
|---|---|---|---|---|---|---|---|---|---|---|---|---|---|---|
| Climate Anomalies | | | LIA | | MWP | | DACP | | | | | | | |
| COSL43 | | | | | | | | | | | | | | |
| COSL47 | | | | | | | | | | | | | | |
| COSL46 | | | | | | | | | | | | | | |
| COSL45 | | | | | | | | | | | | | | |
| COSL51 | | | | | | | | | | | | | | |
| COSL50 | | | | | | | | | | | | | | |
| COSL44 | | | | | | | | | | | | | | |
| COSL49 | | | | | | | | | | | | | | |
| Delaware | | | | | | | | | | | | | | |
| New Jersey | | | | | | | | | | | | | | |
| North Carolina | | | | | | | | | | | | | | |
| South Carolina | | | | | | | | | | | | | | |
| Maine | | | | | | | | | | | | | | |
| Massachusetts | | | | | | | | | | | | | | |
| Bermuda | | | | | | | | | | | | | | |
| Puerto Rico/Bahamas | | | | | | | | | | | | | | |
| Iceland | | | | | | | | | | | | | | |
| NW Mediterranean | | | | | | | | | | | | | | |
| NW France | | | | | | | | | | | | | | |
| | 2017-1817 | 1817-1617 | 1617-1417 | 1417-1217 | 1217-1017 | 1017-817 | 817-617 | 617-417 | 417-217 | 217-17 | 17-183 | 183-383 | 383-583 | 583-783 |

Age (CE)                                                                 Age (BCE)

*Figure 24. Late-Holocene Atlantic storm record periodicity (blue) with Cape Henlopen OSL ages (red). Time segments are in years before OSL measurement, 2017. Segments 0.2-0.7 and 1.3-2.0 ka (shaded tan) show high concurrence between storm records in each region as well as Cape Henlopen OSL ages. The ranges for the Little Ice Age (LIA), Medieval Warm Period (MWP), and Dark Ages Cold Period (DACP) are included. References for storm data: Delaware (Nikitina et al., 2014); New Jersey (Donnelly et al., 2001); North Carolina (Culver et al., 2007; Timmons et al., 2010; Mallinson et al., 2011); South Carolina (Wright et al., 2018); Maine (Buynevich et al., 2007); Massachusetts (Donnelly et al., 2015); Bermuda (Van Hengstum et al., 2015); Puerto Rico (Donnelly and Woodruff, 2007); Bahamas (Van Hengstum et al., 2014; Toomey et al., 2012); Iceland (Jackson et al., 2005); NW Mediterranean (Sabatier et al., 2012); NW France (Sorrel et al., 2009, 2012).*

# 7    Conclusion

Ground penetrating radar (GPR) and optically stimulated luminescence (OSL) dating has unveiled a complex evolutionary history of the Cape Henlopen spit features. The GPR data show consistent facies and facies boundaries throughout Cape Henlopen. In areas where GPR penetration was deep enough, a boundary was visible at -10 m separating what is interpreted as shallow marine sediments below and spit platform sediments above. Another consistent boundary was visible between -4 and -5 m separating what is interpreted as spit platform sediments below and spit beach and dune sediments above. Plotting this boundary elevation against age suggests that the spit platform surface elevation may not be as dependent on sea level as previously though, or there are other external factors that have significant influence of the elevation of the boundary. Overwash fan foresets were quite common throughout the recurved spits as well as the beach accretion plain. These deposits, as well as occasional channel and channel fill features, indicate prevalent storm activity.

The OSL ages reveal a clustering of ages in the relict recurved spits. When plotted against distance the OSL ages reveal a period of rapid growth, indicating that the Cape Henlopen spit complex experienced episodic growth. Recent studies have proposed storms as viable mechanisms for spit growth. In the case of Cape Henlopen, it is likely that storms and storm surges erode updrift sediment sources, thus placing massive amounts of sediment into the littoral system to be deposited on the spit. To see if the Cape Henlopen spit growth corresponded to storm activity, the Cape Henlopen OSL ages were plotted with data from numerous storm records from throughout the North Atlantic basin. This revealed two time periods (0.2-0.7 ka and 1.3-2.0 ka) with significant

correspondence between the Cape Henlopen OSL ages and North Atlantic storm activity. In addition, these two time periods align with the Little Ice Age (LIA) and Dark Ages Cold Period (DACP) climate anomalies. Both the LIA and DACP are associated with increased storm activity in the Western North Atlantic.

This case study provides evidence that the Cape Henlopen spit experienced episodic growth and was likely significantly influenced by storm activity. More case studies in different coastal environments are required to determine if storm influence is a significant external force in the evolution of spits and if other spits experience episodic growth phases that align with North Atlantic storm records.

# 8    References

Aitken, M. J. (1998). An Introduction to Optical Dating: The Dating of Quaternary Sediments by the Use of Photon-stimulated Luminescence. New York, NY: Oxford University Press.

Aitken, M. J. (1985). *Thermoluminescence Dating*. Academic Press.

Allard, J., Bertin, X., Chaumillon, E., & Pouget, F. (2008). Sand spit rhythmic development: A potential record of wave climate variations? Arçay Spit, western coast of France. *Marine Geology*, *253*(3–4), 107–131. https://doi.org/10.1016/j.margeo.2008.05.009

Andrade, C., Freitas, M. C., Moreno, J., & Craveiro, S. C. (2004). Stratigraphical evidence of Late Holocene barrier breaching and extreme storms in lagoonal sediments of Ria Formosa, Algarve, Portugal. *Marine Geology*, *210*(1–4), 339–362. https://doi.org/10.1016/j.margeo.2004.05.016

Andrade, C., Trigo, R. M., Freitas, M. C., Gallego, M. C., Borges, P., & Ramos, A. M. (2008). Comparing historic records of storm frequency and the North Atlantic Oscillation (NAO) chronology for the Azores region. *Holocene*, *18*(5), 745–754. https://doi.org/10.1177/0959683608091794

Ashton, A., Murray, A. B., & Arnault, O. (2001). Formation of coastline features by large-scale instabilities induced by high-angle waves. *Nature*, *414*(6861), 296–300. https://doi.org/10.1038/35104541

Ashton, A. D., & Murray, A. B. (2006a). High-angle wave instability and emergent shoreline shapes: 1. Modeling of sand waves, flying spits, and capes. *Journal of Geophysical Research: Earth Surface*, *111*(4), 1–19. https://doi.org/10.1029/2005JF000422

Ashton, A. D., & Murray, A. B. (2006b). High-angle wave instability and emergent shoreline shapes: 2. Wave climate analysis and comparisons to nature. *Journal of Geophysical Research: Earth Surface*, *111*(4), 1–17. https://doi.org/10.1029/2005JF000423

Ashton, A. D., Nienhuis, J., & Ells, K. (2016). On a neck, on a spit: Controls on the shape of free spits. *Earth Surface Dynamics*, *4*(1), 193–210. https://doi.org/10.5194/esurf-4-193-2016

Aubrey, D. G., & Gaines, A. G. (1982). Rapid formation and degradation of barrier spits in areas with low rates of littoral drift. *Marine Geology*, *49*(3–4), 257–277.

Avinash, K., Deepika, B., & Jayappa, K. S. (2013). Evolution of spit morphology: A case study using a remote sensing and statistical based approach. *Journal of Coastal Conservation*, *17*(3), 327–337. https://doi.org/10.1007/s11852-013-0259-y

Bond, G., Showers, W., Cheseby, M., Lotti, R., Almasi, P., DeMenocal, P., … Bonani, G. (1997). A Pervasive Millennial-Scale Cycle in North Atlantic Holocene and Glacial Climates. *Science*, *278*(5341), 1257–1266. https://doi.org/10.1126/science.278.5341.1257

Bond, G., Kromer, B., Beer, J., Muscheler, R., Evans, M. N., Showers, W., … Bonani, G. (2001). Persistent solar influence on north atlantic climate during the Holocene. *Science*, *294*(5549), 2130–2136. https://doi.org/10.1126/science.1065680

Bradley, R. S., & Jones, P. D. (1992). When was the "Little Ice Age"? In T. Mikami (Ed.), *Proceedings of the International Symposium on the Little Ice Age Climate* (pp. 1–4). Hachioji, Japan: Department of Geography, Tokyo Metropolitan University.

Bradley, R. S., & Jones, P. D. (1993). "Little Ice Age" summer temperature variations: their nature and relevance to recent global warming trends. *The Holocene*, *3*(4), 367–376.

Bristow, C. S., Neil Chroston, P., & Bailey, S. D. (2000). The structure and development of foredunes on a locally prograding coast: Insights from ground-penetrating radar surveys, Norfolk, UK. *Sedimentology*, *47*(5), 923–944. https://doi.org/10.1046/j.1365-3091.2000.00330.x

Bruun, P. (1981). Forms of Equilibrium of Coasts with a Littoral Drift. *Institute of Engineering Research Waves Research Laboratory Technical Report*, *3*(347).

Buynevich, I. V., FitzGerald, D. M., & Goble, R. J. (2007). A 1500 yr record of North Atlantic storm activity based on optically dated relict beach scarps. *Geology*, *35*(6), 543–546. https://doi.org/10.1130/G23636A.1

Costas, S., Alejo, I., Rial, F., Lorenzo, H., & Nombela, M. A. (2006). Cyclical Evolution of a Modern Transgressive Sand Barrier in Northwestern Spain Elucidated by GPR and Aerial Photos. *Journal of Sedimentary Research*, *76*(9), 1077–1092. https://doi.org/10.2110/jsr.2006.094

Costas, S., & FitzGerald, D. (2011). Sedimentary architecture of a spit-end (Salisbury Beach, Massachusetts): The imprints of sea-level rise and inlet dynamics. *Marine Geology*, *284*(1–4), 203–216. https://doi.org/10.1016/j.margeo.2011.04.002

Costas, S., Rebêlo, L., Brito, P., Burbidge, C. I., Prudêncio, M. I., FitzGerald, D. (Editors) (2015). *Sand and Gravel Spits* (Vol. 12).

Culver, S. J., Grand Pre, C. A., Mallinson, D. J., Riggs, S. R., Corbett, D. R., Foley, J., … Twamley, D. (2007). Late Holocene barrier island collapse: Outer Banks, North Carolina, USA. *The Sedimentary Record*, *5*(4), 4–8.

Cunningham, A. C., & Wallinga, J. (2010). Selection of integration time intervals for quartz OSL decay curves. *Quaternary Geochronology*, *5*(6), 657–666. https://doi.org/10.1016/j.quageo.2010.08.004

Daly, J., McGreary, S., & Krantz, D. E. (2002). Ground-penetrating radar investigation of a late Holocene spit complex: Cape Henlopen, Delaware. *Journal of Coastal Research*, *18*(2), 274–286.

Davis, J. L., & Annan, a. P. (1989). Ground-Penetrating Radar for High-Resolution Mapping of Soil and Rock Stratigraphy. *Geophysical Prospecting*, (May 1988), 531–551. https://doi.org/10.1111/j.1365-2478.1989.tb02221.x

Davis, W. M. (1896). The Outline of Cape Cod. *Proceedings of the American Academy of Arts and Sciences*, *31*(May), 303–332.

Davis, R. E., & Dolan, R. (1992). The "All Hallows'' Eve" Coastal Storm - October 1991." *Coastal Research*, *8*(4), 978–983.

Davis, R. E., & Dolan, R. (1993). Nor'easters. *American Scientist*, *81*(5), 428–439. Retrieved from https://www.uvm.edu/cosmolab/papersX/Davis_1993_4200.pdf

Donnelly, J. P., Roll, S., Wengren, M., Butler, J., Lederer, R., & Webb, T. (2001). Sedimentary evidence of intense hurricane strikes from New Jersey. *Geology*, *29*(7), 615–618. https://doi.org/10.1130/0091-7613(2001)029<0615:SEOIHS>2.0.CO;2

Donnelly, J. P., & Woodruff, J. D. (2007). Intense hurricane activity over the past 5,000 years controlled by El Ni??o and the West African monsoon. *Nature*, *447*, 465–468. https://doi.org/10.1038/nature05834

Donnelly, J., Hawkes, A. D., Lane, P., Macdonald, D., Shuman, B. N., Toomey, M. R., … Woodru, J. D. (2015). Climate forcing of unprecedented intense-hurricane activity in the last 2000 years. *AGU Publications*, 49–65. https://doi.org/10.1002/2014EF000274.Received

Dougherty, A. J., Fitzgerald, D. M., & Buynevich, I. V. (2004). Evidence for storm-dominated early progradation of Castle Neck barrier, Massachusetts, USA. *Marine Geology*, *210*(1–4), 123–134. https://doi.org/10.1016/j.margeo.2004.05.006

Dougherty, A. J., Choi, J.-H., & Dosseto, A. (2016). Prograded Barriers plus GPR plus OSL = Insight on Coastal Change over Intermediate Spatial and Temporal Scales. *Journal of Coastal Research*, *75*(SI), 368–372. https://doi.org/10.2112/si75-074.1

Duller, G. A. T. (2008). Luminescence Dating: Guidelines on using luminescence dating in archaeology. *Swindon: English Heritage*, 1–44. https://doi.org/10.1002/jqs.1328

Evans, O. F. (1939). Mass Transportation of Sediments on Subaqueous Terraces. *Journal of Geology*, *47*(1938), 325–334. https://doi.org/10.1086/624781

Fruergaard, M., Møller, I., Johannessen, P. N., Nielsen, L. H., Andersen, T. J., Nielsen, L., … Pejrup, M. (2015). Stratigraphy, Evolution, and Controls of A Holocene Transgressive–Regressive Barrier Island Under Changing Sea Level: Danish North Sea Coast. *Journal of Sedimentary Research*, *85*(7), 820–844. https://doi.org/10.2110/jsr.2015.53

Dougherty, A. J., Choi, J.-H., & Dosseto, A. (2016). Prograded Barriers plus GPR plus OSL = Insight on Coastal Change over Intermediate Spatial and Temporal Scales. *Journal of Coastal Research*, *75*(SI), 368–372. https://doi.org/10.2112/si75-074.1

Duller, G. A. T. (2008). Luminescence Dating: Guidelines on using luminescence dating in archaeology. *Swindon: English Heritage*, 1–44. https://doi.org/10.1002/jqs.1328

Galbraith, R. F., Roberts, R. G., Laslett, G. M., Yoshida, H., Olley, J. M., Galbraith, R. F., … Laslett, G. M. (1999). Optical dating of single and multiple grains of quartz from Jinmium rock shelter, Northern Australia: Part I, Experimetal design and statistical models. *Archaeometry*, *41*(2), 339–364. https://doi.org/10.1111/j.1475-4754.1999.tb00987.x

Galgano Jr, F. A. (2008). Shoreline behavior along the Atlantic coast of Delaware. *Middle States Geographer*, *41*, 74–81. Retrieved from http://msaag.org/wp-content/uploads/2013/04/10_Galgano.pdf

Gilbert, G. K. (1885). *The Topographic Features of Lake Shores*. U.S. Government Printing Office.

Guérin, G., Mercier, N., Nathan, R., Adamiec, G., & Lefrais, Y. (2012). On the use of the infinite matrix assumption and associated concepts: A critical review. *Radiation Measurements*, *47*(9), 778–785. https://doi.org/10.1016/j.radmeas.2012.04.004

Gulliver, F. P. (1899). Shoreline Topography. *Proceedings of the American Academy of Arts and Sciences*, *34*(8), 151–258.

Hayes, M. O. (1980). General morphology and sediment patterns in tidal inlets. *Sedimentary Geology*, *26*(1–3), 139–156. https://doi.org/10.1016/0037-0738(80)90009-3

Hayes, M. O. (1979). Barrier island morphology as a function of tidal and wave regime. In: Leatherman, S.P. (Ed.). *Academic Press*, (July), 1–27.

Hayes, M. O. (Editor) (1969). Coastal Environments: NE Massachusetts and New Hampshire. Field Trip for Eastern Section of SEPM.

Helama, S., Jones, P. D., & Briffa, K. R. (2017). Dark Ages Cold Period: A literature review and directions for future research. *Holocene*, *27*(10), 1600–1606. https://doi.org/10.1177/0959683617693898

Héquette, A., & Ruz, M. H. (1991). Spit and Barrier-Island Migration in the Southeastern Canadian Beaufort Sea. *Journal of Coastal Research*, *7*(3), 677–698.

Hine, A. C. (1979). Mechanisms of berm development and resulting beach growth along a barrier spit complex. *Sedimentology*, *26*(3), 333–351. https://doi.org/10.1111/j.1365-3091.1979.tb00913.x

Houser, C., & Greenwood, B. (2007). Onshore Migration of a Swash Bar During a Storm. *Journal of Coastal Research*, *231*(231), 1–14. https://doi.org/10.2112/03-0135.1

Huntley, D. J., Godfrey-Smith, D. I., & Thewalt, M. L. W. (1985). Optical dating of sediments. *Nature*, *313*, 105–107. https://doi.org/10.1038/316507a0

Hurrell, J. W., Kushnir, Y., Otterson, G., & Visbeck, M. (2003). An Overview of the North Atlantic Oscillation. *The North Atlantic Oscillation: Climatic Significance and Environmental Impact*, *134*, 263. https://doi.org/10.1029/GM134

Hurrell, J. W., & Deser, C. (2009). North Atlantic climate variability: The role of the North Atlantic Oscillation. *Journal of Marine Systems*, *78*, 28–41. https://doi.org/10.1007/s00382-016-3502-z

Imperato, D. P., Sexton, W. J., & Hayes, M. O. (1988). Stratigraphy and sediment characteristics of a mesotidal ebb-tidal delta, North Edisto Inlet, South Carolina. *Journal of Sedimentary Research*, *58*(6), 950–958. https://doi.org/10.1306/212f8ec7-2b24-11d7-8648000102c1865d

Jackson, M. G., Oskarsson, N., Trønnes, R. G., McManus, J. F., Oppo, D. W., Grönvold, K., … Sachs, J. P. (2005). Holocene loess deposition in Iceland: Evidence for millenial-scale atmosphere-ocean coupling in the North Atlantic. *Geology*, *33*(6), 509–512. https://doi.org/10.1130/G21489.1

Jelgersma, S., Stive, M. J. F., & van der Valk, L. (1995). Holocene storm surge signatures in the coastal dunes of the western Netherlands. *Marine Geology*, *125*(1–2), 95–110. https://doi.org/10.1016/0025-3227(95)00061-3

Jiménez, J. A., & Sánchez-Arcilla, A. (2004). A long-term (decadal scale) evolution model for microtidal barrier systems. *Coastal Engineering*, *51*(8–9), 749–764. https://doi.org/10.1016/j.coastaleng.2004.07.007

Johnson, D. W. (1919). *Shoreline Processes and Development*. New York: John Wiley & Sons.

Kana, T. W., Hayter, E. J., & Work, P. a. (1999). Mesoscale Sediment Transport at Southeastern U.S. Tidal Inlets: Conceptual Model Applicable to Mixed Energy Settings. *Journal of Coastal Research*, *15*(2), 303–313. Retrieved from http://www.jstor.org/stable/4298943

Keigwin, L. D. (1996). The Little Ice Age and Medieval Warm Period in the Sargasso Sea. *Science*, *274*(5292), 1503–1508. https://doi.org/10.1126/science.274.5292.1503

Keim, B. D., Muller, R. A., & Stone, G. W. (2004). Spatial and temporal variability of coastal storms in the North Atlantic Basin. *Marine Geology*, *210*(1–4), 7–15. https://doi.org/10.1016/j.margeo.2003.12.006

King, C. A. M., & McCullagh, M. J. (1971). A simulation model of a complex recurved spit. *The Journal of Geology*, *79*(1), 22–37.

Komar, P. D. (1971). The mechanics of sand transport on beaches. *Journal of Geophysical Research*, *76*(3), 713–721. https://doi.org/10.1029/JC076i003p00713

Kraft, J. C. (1971). Sedimentary environment, facies pattern, and geologic history of a Holocene marine transgression. *Geological Society America Bulletin*, *82*(August), 2131–2158. https://doi.org/10.1130/0016-7606(1971)82[2131:SFPAGH]2.0.CO;2

Kraft, J. C., Allen, E. A., & Maurmeyer, E. (1978). The geological and paleogeomorphological evolution of a spit system and its associated coastal environments: Cape Henlopen Spit, Delaware. *Journal of Sedimentary Petrology*, *48*(1), 211–225. https://doi.org/10.1306/212F7437-2B24-11D7-8648000102C1865D

Kraft, J. C., & Hiller, A. V. (1987). Cape Henlopen spit: A late Holocene sand accretion complex at the mouth of the Delaware Bay, Delaware. *North-Eastern Section of the Geological Society of America: Decade of North American Geology, Centennial Field Guides,5*, 19-22.

Lang, A., Hatte, C., Rousseau, D. D., Antoine, P., Fontugne, M., Zoller, L., and Hambach, U., 2003, High-resolution chronologies for loess: comparing AMS C-14 and optical dating results. *Quaternary Science Reviews*, v. 22, no. 10-13, p. 953-959.

Leatherman, S. P. (1979). Migration of Assateague Island, Maryland, by inlet and overwash processes. *Geology*, *7*, 104–107.

Lindhorst, S., Betzler, C., & Hass, H. C. (2008). The sedimentary architecture of a Holocene barrier spit (Sylt, German Bight): Swash-bar accretion and storm erosion. *Sedimentary Geology*, *206*(1–4), 1–16. https://doi.org/10.1016/j.sedgeo.2008.02.008

Lindhorst, S., Fürstenau, J., Christian Hass, H., & Betzler, C. (2010). Anatomy and sedimentary model of a hooked spit (Sylt, southern North Sea). *Sedimentology*, *57*(4), 935–955. https://doi.org/10.1111/j.1365-3091.2009.01126.x

Liu, K. B., & Fearn, M. L. (2000). Reconstruction of prehistoric landfall frequencies of catastrophic hurricanes in Northwestern Florida from lake sediment records. *Quaternary Research*, *54*(2), 238–245. https://doi.org/10.1006/qres.2000.2166

Lund, D. C., Lynch-Stieglitz, J., & Curry, W. B. (2006). Gulf Stream density structure and transport during the past millennium. *Nature*, *444*(7119), 601–604. https://doi.org/10.1038/nature05277

Mailier, P. J., Stephenson, D. B., Ferro, C. A. T., & Hodges, K. I. (2006). Serial Clustering of Extratropical Cyclones. *Monthly Weather Review*, *134*, 2224–2240.

Mallinson, D. J., Smith, C. W., Culver, S. J., Riggs, S. R., & Ames, D. (2010). Geological characteristics and spatial distribution of paleo-inlet channels beneath the outer banks barrier islands, North Carolina, USA. *Estuarine, Coastal and Shelf Science*, *88*(2), 175–189. https://doi.org/10.1016/j.ecss.2010.03.024

Mallinson, D. J., Smith, C. W., Mahan, S., Culver, S. J., & McDowell, K. (2011). Barrier island response to late Holocene climate events, North Carolina, USA. *Quaternary Research*, *76*(1), 46–57. https://doi.org/10.1016/j.yqres.2011.05.001

Malvern Ltd. (2015). *A basic guide to particle characterization*. Retrieved from http://www.malvern.com

Mann, M. E. (2009). Medieval Climate Anomaly. *Science*, *78*(November), 1256–1260. https://doi.org/10.1126/science.1166349

Mann, M. E., Woodruff, J. D., Donnelly, J. P., & Zhang, Z. (2009). Atlantic hurricanes and climate over the past 1,500 years. *Nature*, *460*(7257), 880–883. https://doi.org/10.1038/nature08219

Matthews, J. A., & Briffa, K. R. (2005). The "Little Ice Age": Re-evaluation of an evolving concept. *Geografiska Annaler, Series A: Physical Geography*, *87*(1), 17–36. https://doi.org/10.1111/j.0435-3676.2005.00242.x

Maurmeyer, E. M. (1974). *Analysis of Short- and Long-term Elements of Coastal Change in a Simple Spit System: Cape Henlopen, Delaware*. Newark, DE: University of Delaware.

Mayewski, P. A., Rohling, E. E., Stager, J. C., Karlén, W., Maasch, K. A., Meeker, L. D., … Steig, E. J. (2004). Holocene climate variability. *Quaternary Research*, *62*, 243–255. https://doi.org/10.1016/j.yqres.2004.07.001

Meistrell, F. J., 1972, The spit-platform concept: laboratory observation of spit development, *in* Schwartz, M., ed., *Spits and Bars: Benchmark Papers in Geology*: Stroudsburg, Pennsylvania, Dowden, Hutchinson and Ross, p. 225-283.

McKeever, S. W. S. (2001). Optically stimulated luminescence dosimetry. *Nuclear Instruments and Methods in Physics Research*, *184*, 65.

Montes, A., Bujalesky, G. G., & Paredes, J. M. (2018). *Geomorphology and internal architecture of Holocene sandy-gravel beach ridge plain and barrier spits at Río Chico area, Tierra del Fuego, Argentina*. *Journal of South American Earth Sciences* (Vol. 84). Elsevier Ltd. https://doi.org/10.1016/j.jsames.2018.03.012

Moslow, T. F., & Heron, S. D. (1978). Relict inlets; preservation and occurrence in the Holocene stratigraphy of southern core banks, North Carolina. *Journal of Sedimentary Research*, *48*(4), 1275–1286. https://doi.org/10.1306/212f765d-2b24-11d7-8648000102c1865d

Murray, A. S., and Roberts, R. G., 1997, Determining the burial time of single grains of quartz using optically stimulated luminescence. *Earth and Planetary Science Letters*, v. 152, no. 1-4, p. 163-180.

Murray, A. S., & Wintle, A. G. (2000). Luminescence dating of quartz using an improved single-aliquot regenerative-dose protocol. *Radiation Measurements*, *32*, 57–73.

Murray, A. S., & Wintle, A. G. (2003). The single aliquot regenerative dose protocol: Potential for improvements in reliability. *Radiation Measurements*, *37*(4–5), 377–381. https://doi.org/10.1016/S1350-4487(03)00053-2

Neal, A., 2004, Ground-penetrating radar and its use in sedimentology: principles, problems and progress. *Earth-Science Reviews*, v. 66, no. 3, p. 261-330.

Nikitina, D. L., Kemp, A. C., Horton, B. P., Vane, C. H., van de Plassche, O., & Engelhart, S. E. (2014). Storm erosion during the past 2000years along the north shore of Delaware Bay, USA. *Geomorphology*, *208*, 160–172. https://doi.org/10.1016/j.geomorph.2013.11.022

NOAA. (2017). Is sea level rising? Retrieved September 21, 2017, from https://oceanservice.noaa.gov/facts/sealevel.html

Noren, A. J., Bierman, P. R., Steig, E. J., Lini, A., & Southon, J. (2002). Millennial-scale storminess variability in the northeastern United States during the Holocene epoch. *Nature*, *419*(6909), 821–824. https://doi.org/10.1038/nature01132

O'Brien, S. R., Mayewski, P. A., Meeker, L. D., Meese, D. A., Twickler, M. S., & Whitlow, S. (1995). Complexity of Holocene Climate as Reconstructed from a Greenland Ice Core. *Science*, *270*(21), 1962–1964.

Olsen, J., Anderson, N. J., & Knudsen, M. F. (2012). Variability of the North Atlantic Oscillation over the past 5,200 years. *Nature Geoscience*, *5*(11), 808–812. https://doi.org/10.1038/ngeo1589

Petersen, D., Deigaard, R., & Fredsøe, J. (2008). Modelling the morphology of sandy spits. *Coastal Engineering*, *55*(7–8), 671–684. https://doi.org/10.1016/j.coastaleng.2007.11.009

Pierce, J. W. (1970). Tidal Inlets and Washover Fans. *The Journal of Geology*, *78*(2), 230–234. https://doi.org/10.1086/627504

Prescott, J. R., & Hutton, J. T. (1994). Cosmic ray contributions to dose rates for luminescence and ESR dating: Large depths and long-term time variations. *Radiation Measurements*, *23*(2–3), 497–500. https://doi.org/10.1016/1350-4487(94)90086-8

Preusser, F., Degering, D., Fuchs, M., Hilgers, A., Kadereit, A., Klasen, N., … Spencer, J. Q. G. (2008). Luminescence dating: basics, methods and applications. *Eiszeitalter Und Gegenwart Quaternary Science Journal*, *57*(1–2), 95–149. https://doi.org/http://dx.doi.org/10.3285/eg.57.1-2.5

Ramsey, K. W. (1999a). Cross Section of Pliocene and Quaternary Deposits Along the Atlantic Coast of Delaware. Newark: Delaware Geological Survey.

Ramsey, K. W. (1999b). Beach Sand Textures from the Atlantic Coast of Delaware. *Delaware Geological Survey Open File Report No. 41*, (41).

Ramsey, K. W., & Baxter, S. J. (1996). Radiocarbon dates from Delaware: A compilation. *Delaware Geological Survey Report of Investigations*, *54*.

Rhodes, E. J. (2011). Optically Stimulated Luminescence Dating of Sediments over the Past 200,000 Years. *Annual Review of Earth and Planetary Sciences*, *39*(1), 461–488. https://doi.org/10.1146/annurev-earth-040610-133425

Rink, W. J., & López, G. I. (2010). OSL-based lateral progradation and aeolian sediment accumulation rates for the Apalachicola Barrier Island Complex, North Gulf of Mexico, Florida. *Geomorphology*, *123*(3–4), 330–342. https://doi.org/10.1016/j.geomorph.2010.08.001

Rodnight, H., Duller, G. A. T., Tooth, S., and Wintle, A. G., 2005, Optical dating of a scroll-bar sequence on the Klip River, South Africa, to derive the lateral migration rate of a meander bend. *Holocene*, v. 15, no. 6, p. 802-811.

Sabatier, P., Dezileau, L., Colin, C., Briqueu, L., Bouchette, F., Martinez, P., … Von Grafenstein, U. (2012). 7000 years of paleostorm activity in the NW Mediterranean Sea in response to Holocene climate events. *Quaternary Research*, *77*(1), 1–11. https://doi.org/10.1016/j.yqres.2011.09.002

Scheffers, A., Engel, M., Scheffers, S., Squire, P., & Kelletat, D. (2012). Beach ridge systems - archives for holocene coastal events? *Progress in Physical Geography*, *36*(1), 5–37. https://doi.org/10.1177/0309133311419549

Schwartz, M. L. (1972). *Spits & Bars* (1st ed.). Dowden, Hutchinson & Ross, Inc.

Schwartz, R. K. (1982). Bedform and stratification characteristics of some modern small-scale washover sand bodies. *SedimentologySchwartz, R. K. (1982). Bedform and Stratification Characteristics of Some Modern Small-Scale Washover Sand Bodies. Sedimentology, 29, 835–849.*, *29*, 835–849.

Shaffrey, L., & Sutton, R. (2006). Bjerknes Compensation and the Decadal Variability of the Energy Transports in a Coupled Climate Model. *Journal of Climate*, *19*(1964), 1167–1181. https://doi.org/10.1175/JCLI3652.1

Shen, Z., Mauz, B., and Lang, A., 2011, Source-trap characterization of thermally transferred OSL in quartz. *Journal of Physics D: Applied Physics*, v. 44, no. 29, p. 295405.

Shen, Z., and Mauz, B., 2012, Optical dating of young deltaic deposits on a decadal time scale. *Quaternary Geochronology*, v. 10, p. 110-116.

Simms, A. R., Anderson, J. B., & Blum, M. (2006). Barrier-island aggradation via inlet migration: Mustang Island, Texas. *Sedimentary Geology*, *187*(1–2), 105–125. https://doi.org/10.1016/j.sedgeo.2005.12.023

Sorrel, P., Debret, M., Billeaud, I., Jaccard, S. L., McManus, J. F., & Tessier, B. (2012). Persistent non-solar forcing of Holocene storm dynamics in coastal sedimentary archives. *Nature Geoscience*, *5*(12), 892–896. https://doi.org/10.1038/ngeo1619

Sorrel, P., Tessier, B., Demory, F., Delsinne, N., & Mouazé, D. (2009). Evidence for millennial-scale climatic events in the sedimentary infilling of a macrotidal estuarine system, the Seine estuary (NW France). *Quaternary Science Reviews*, *28*(5–6), 499–516. https://doi.org/10.1016/j.quascirev.2008.11.009

Tamura, T., Saito, Y., Bateman, M. D., Nguyen, V. L., Ta, T. K. O., & Matsumoto, D. (2012). Luminescence dating of beach ridges for characterizing multi-decadal to

centennial deltaic shoreline changes during Late Holocene, Mekong River delta. *Marine Geology*, *326–328*, 140–153. https://doi.org/10.1016/j.margeo.2012.08.004

Thomas, T., Lynch, S. K., Phillips, M. R., & Williams, A. T. (2014). Long-term evolution of a sand spit, physical forcing and links to coastal flooding. *Applied Geography*, *53*, 187–201. https://doi.org/10.1016/j.apgeog.2014.06.020

Tillmann, T. (2012). Ground-penetrating radar in coastal environments: Examples from the islands Sylt and Amrum. *Bremer Beiträge Zur Geographie U. Raumplanung*, (44), 60–77.

Tillmann, T., & Wunderlich, J. (2011). Facies and Development of a Holocene Barrier Spit (Southern Sylt/German North Sea). In *2011 6th International Workshop on Advanced Ground Penetrating Radar (IWAGPR)* (pp. 1–7). Aachen: IEEE. https://doi.org/10.1109/IWAGPR.2011.5963874

Tillmann, T., & Wunderlich, J. (2013). Barrier rollover and spit accretion due to the combined action of storm surge induced washover events and progradation: Insights from ground-penetrating radar surveys and sedimentological data. *Journal of Coastal Research*, *65*, 600–605. https://doi.org/10.2112/SI65-102.1

Timmons, E. A., Rodriguez, A. B., Mattheus, C. R., & DeWitt, R. (2010). Transition of a regressive to a transgressive barrier island due to back-barrier erosion, increased storminess, and low sediment supply: Bogue Banks, North Carolina, USA. *Marine Geology*, *278*(1–4), 100–114. https://doi.org/10.1016/j.margeo.2010.09.006

Toomey, M. R., Curry, W. B., Donnelly, J. P., & Van Hengstum, P. J. (2013). Reconstructing 7000 years of North Atlantic hurricane variability using deep-sea sediment cores from the western Great Bahama Bank. *Paleoceanography*, *28*(1), 31–41. https://doi.org/10.1002/palo.20012

Trouet, V., Esper, J., Graham, N. E., Baker, A., Scourse, J. D., & Frank, D. C. (2009). Persistent positive north atlantic oscillation mode dominated the medieval climate anomaly. *Science*, *324*(5923), 78–80. https://doi.org/10.1126/science.1166349

Van Hengstum, P. J., Donnelly, J. P., Kingston, A. W., Williams, B. E., Scott, D. B., Reinhardt, E. G., … Patterson, W. P. (2015). Low-frequency storminess signal at Bermuda linked to cooling events in the North Atlantic region. *Paleoceanography*, *30*(2), 52–76. https://doi.org/10.1002/2014PA002662

Van Hengstum, P. J., Donnelly, J. P., Toomey, M. R., Albury, N. A., Lane, P., & Kakuk, B. (2014). Heightened hurricane activity on the Little Bahama Bank from 1350 to 1650 AD. *Continental Shelf Research*, *86*(C), 103–115. https://doi.org/10.1016/j.csr.2013.04.032

Van Overmeeren, R. A. (1998). Radar facies of unconsolidated sediments in The Netherlands: A radar stratigraphy interpretation method for hydrogeology. *Journal of Applied Geophysics*, *40*(1–3), 1–18. https://doi.org/10.1016/S0926-9851(97)00033-5

Van Vliet-Lanoë, B., Penaud, A., Hénaff, A., Delacourt, C., Fernane, A., Goslin, J., … Le Cornec, E. (2014). Middle- to late-Holocene storminess in Brittany (NW France): Part II - The chronology of events and climate forcing. *Holocene*, *24*(4), 434–453. https://doi.org/10.1177/0959683613519688

Wintle, A. G., & Murray, A. S. (2006). A review of quartz optically stimulated luminescence characteristics and their relevance in single-aliquot regeneration dating protocols. *Radiation Measurements*, *41*(4), 369–391. https://doi.org/10.1016/j.radmeas.2005.11.001

Wright, E., Kruse, S., Forman, S. L., & Harris, M. S. (2018). Millennial Scale Development of a Southeastern United States Spit. *Journal of Coastal Research*, *342*, 255–271. https://doi.org/10.2112/JCOASTRES-D-16-00005.1

Zenkovitch, V. P., Steers, J. A., & Fry, D. G. (1959). Processes of Coastal Development. *Geographical Review*, *58*(4), 685–687.